Final Draft

of the original manuscript

Lüdmann, T.; Saitz, M.; Metzing, J.; Emeis, K.:

Acoustic backscatter analysis of ground-fishing activity in the German North Sea sector.

In: Continental Shelf Research. Vol. 212 (2021) 104292.

First published online by Elsevier: 05.11.2020

https://dx.doi.org/10.1016/j.csr.2020.104292

Acoustic backscatter analysis of ground-fishing activity in the German North Sea sector

Lüdmann, T.[a,*], Saitz, M.Y.[a], Metzing, J.[a], Emeis, K.-C.[a,b]

[a] University of Hamburg, Center of Geosciences and Sustainability, Institute of Geology, Germany.
[b] Helmholtz Zentrum Geesthacht, Institute of Coastal Research, Germany.

Abstract

The physical impact of demersal fishing was studied in three different areas of the German North Sea sector by use of a multibeam echosounder. The areas represent typical shallow seas siliciclastic habitats in variable distance to the coastline. Their seabed substrate is dominated by coarse silt close to the shore and by fine sand in the most distal area on the Dogger Bank. The study documents the utility of the multibeam as a suitable tool to map large seafloor areas, as well as to quantify and qualify the footprints of the fishing groundgear. Besides the depth and amplitude information, the multibeam data allows the analysis of the incidence angle-dependent variation of the backscatter signal that provides additional information on the seabed impedance, roughness, volume scatter and substrate type. Two main types of destructive seafloor pattern were observed in the three areas. The dominant type are pairs of parallel furrows exhibiting widths of 6–9 m and depths of 2–6 cm and is related to beam trawling. Separation distance of the pair furrows is 16–23 m. The second type are pairs of narrow furrows (3–4 m) with much larger separation distance of 110–120 m. They are attributed to otter board trawling. A comparison of their mechanical ramification shows that the fishing gear incises the seafloor and modifies seafloor structures and properties. Our investigation documents that beam trawling has the greatest physical impact and exhibits the highest furrow density in the three study areas. The created furrows can persist for at least 4 months in a substrate of very fine sand. Depending on the hydrodynamic regime, the furrows can be later refilled by finer sediments, or levelled out by storm wave-induced turbulence reaching the seafloor. The hydrofoils used in otter trawl to spread the net likewise incise the seafloor, but the furrows are much narrower. However, the ground rope of the net towed between the boards scratches the seafloor and levels the microscale topography along track widths of ca. 100 m.

Keywords: multibeam sonar, acoustic backscatter, Angular Range Analysis, ground-fishing, North Sea

* Corresponding author.
E-Mail Address: thomas.luedmann@uni-hamburg.de (T. Lüdmann)
University of Hamburg, Institute of Geology, Bundesstr. 55, 20146 Hamburg

1. Introduction

High resolution maps of coastal and offshore areas, substrates and habitats are in increasing demand for understanding and assessing anthropogenic impacts, as well as for future management planning of these regions. Bottom trawling in particular, a fishing technique that tows nets along the seafloor to harvest bottom dwelling species, has raised concerns about the mechanical impact on seabed habitats and the related negative effects on benthic ecosystems (Jennings and Kaiser, 1998; Watling and Norse, 1998; Kaiser et al., 2002). Bottom trawling causes a significantly higher disturbance of the seafloor than all other offshore human activities combined (Eastwood et al., 2007; Benn et al., 2010) and is affecting wide areas on continental shelfs worldwide. This problem is addressed by the European Marine Strategy Framework Directive through descriptor 6, which focuses on seafloor integrity and highlights the need for indicators of pressures and state for marine management (Rice et al., 2010, 2012). The International Council for the Exploration of the Sea (ICES) asserts a highly aggregated fishing pressure for the Greater North Sea, with a relatively high impact on deeper waters and in muddy habitats (ICES, 2017). Habitat impacts are higher in muddy and mixed sediments as compared to sand and coarse sediments (Rijnsdorp et al., 2017).

Acoustics is increasingly regarded as an appropriate remote sensing tool that will provide the basic background data for classifying and mapping ocean habitats (e.g., Holler et al., 2016). Acoustic responses from the surficial sediments have been shown to contain details about the character of the seabed, e.g. rock or sediment type, grain size distribution, porosity, roughness, material density, and tortuosity (Nafe and Drake, 1964; Morris et al., 1978; Lurton, 2010; Freitas et al., 2006; Fonseca and Mayer, 2007). Accordingly, acoustic echosounding and related technologies are increasingly being used to assess, characterize, and map seabed environments (Hughes et al., 1996; Mayer, 2006; ICES, 2007; Anderson et al., 2008; Brown and Blondel, 2009, Brown et al., 2011; Snellen et al., 2013; Santos et al., 2018).

Acoustics is increasingly regarded as an appropriate remote sensing tool that will provide the basic background data for classifying and mapping ocean habitats (e.g., Holler et al., 2016). Acoustic responses from the surficial sediments have been shown to contain details about the character of the seabed, e.g. rock or sediment type, grain size distribution, porosity, roughness, material density, and tortuosity (Nafe and Drake, 1964; Morris et al., 1978; Freitas et al., 2006; Fonseca and Mayer, 2007; Lurton, 2010). Accordingly, acoustic echosounding and related technologies are increasingly being used to assess, characterize, and map seabed environments (Hughes-Clarke et al., 1996; Mayer, 2006; ICES, 2007; Anderson et al., 2008; Brown and Blondel, 2009; Brown et al., 2011; Snellen et al., 2013; Santos et al., 2018). The aim of this study is to remotely monitor the spatial and temporal impact of bottom-contact fishing on the seabed habitats using a multibeam echosounder (MBES) system. It has the advantage over single-beam echosounder (SBES) and side-scan sonar systems to provide a much higher spatial range and to simultaneously measure the time of the echo return as well as its acoustic backscatter. This allows to utilize the bathymetry and angle-dependent as well as angle–independent contribution of the backscatter signal to derive seafloor properties. To study the angle-dependent backscatter strength we applied the angular range analysis (ARA) method implemented in the Geocoder algorithm that analyses variations of the seabed returns as a function of the incidence angle (Fonseca et al., 2005; Fonseca and Mayer, 2007). There are other methods to exploit the angular dependence of the acoustic backscatter (e.g. Alevizos et al., 2018) but we selected the Geocoder tool because it is an integral part of the software from Quality Positioning Services (QPS) that concurrently computes backscatter mosaics and ARA

derivates (impedance, roughness, mean grain-size and volume scatter). In addition, it has been successfully applied for seafloor characterization of siliciclastic substrates in the scope of several hydroacoustic studies (Fonseca and Mayer, 2007; Fonseca et al., 2009; Santos et al., 2018). Moreover, its derived sediment properties correlate well with our ground-truth data on discrete sediment samples and video observations. Remote seafloor characterization systems are prone to error in substrates of mixed origin and are sensitive to abundance of shell fragments or to the occurrence of benthic and epibenthic fauna and flora. On the other hand, we here show the potential of the MBES system to investigate the impact of bottom fishing on the seafloor habitats and to document the necessity of obtaining multiple seafloor properties instead of only relying on bathymetry and backscatter strength for the analysis.

The areas of interest are located within the German Exclusive Economic Zone of the North Sea and were surveyed with the RV Heincke between 2013 and 2016 under the framework of the NOAH project (North Sea - Observation and Assessment of Habitats). Nine dedicated areas with a box size of 10 × 10 km were chosen that present typical seafloor habitats (Fig. 1). In this study, we focus on three of these areas (NOAH D, G and I) that reveal a range of inner and middle shelf conditions and different fishing intensities.

2. Setting

North Sea habitats

The North Sea is a shallow epicontinental sea on the European continental shelf connected to the Atlantic Ocean via the English Channel in the south and the Norwegian Sea in the north. It is located between the European mainland including Germany, the Netherlands, Belgium, France and Scandinavia as well as Great Britain. This epeiric sea is over 970 km long by 580 km wide at its maximum extent and has an area of ca. 750,000 km2 (Fig. 1A). The NOAH working areas are located in considerably different distance to the shoreline, in the sublittoral zone of the North Sea. NOAH I is located at the eastern edge of the Dogger Bank, NOAH G at the eastern flank of the Elbe glacial valley and NOAH D 40 km off the East Frisian Islands (Fig. 1B). The Dogger Bank forms an NE-SW-trending elevated platform (100 km wide, 300–350 km long) that consists of Pleistocene deposits overlain by modern sands (Stride, 1959; Von Haugwitz and Wong, 1988; Cameron et al., 1992). Because it is shallow and flat, the top of the bank is exposed to turbulent hydrodynamic conditions (disturbances), whereas more stable conditions prevail at its slopes (Van Moorsel, 2011). Recognizable bedforms are present down to a water depth of approximately 50 m. They consist mainly of sand streaks and ripples. Waves of coarse sand and gravel are locally present (Diesing et al., 2009). Bottom current flow is affected by the M2 tidal cycle with predominant directions of southeast and northwest (Otto et al., 1990). For the period 1970–1999, a mean current velocity 1 m above bottom of 16.6 cms 1 was modeled, with maximum values of 73 cm s 1 (NOAH, 2020). The modeled average maximum bed shear stress generated by the combined action of waves and currents for the time period 1984–2015 in the southern North Sea lies in the range of 0.45–0.04 N m 2 (NOAH, 2020).

NOAH G represents conditions in the postglacial sediment fill of the Elbe glacial valley that forms a NW to SE striking glacial structure. It lies ca. 120 km westward of the Island Sylt on flat seabed in water depths of 44–46 m that gently rises eastward to the ground moraine region. Bottom current flow is characterized by the M2 tidal cycle (Otto et al., 1990). The mean modeled current velocity 1 m above bottom for the period 1970–1999 is 19.9 cm s 1 whereby

the highest value reaches 61 cm s 1 (NOAH, 2020). Seasonal differences between the maximum currents point to an influence of wind induced currents in NOAH G. However, the tidal forces dominate the current regime. The average maximum bed shear stress is in the range of 0.22–0.04 N m 2 (NOAH, 2020). The inner shelf site NOAH D is located in a water depth of ca. 35 m, in the near reach of the Ems, Jade and Weser Rivers. It represents conditions in the mobile coast-parallel sand belt. Near-bottom current velocity is influenced by the M2 tidal cycle (Otto et al., 1990). Mean current velocity 1 m above bottom for the period 1970–1999 is 31.8 cm s 1 with maximum values of 77 cm s 1 (NOAH, 2020). Minor seasonal variations in current speed denote the subsequent role of wind-driven currents. The average maximum bed shear stress is computed to 0.2–0.07 N m 2 (NOAH, 2020).

Bottom Trawling

The North Sea has been intensively trawled for decades and is a major fishing ground for the eight bordering countries and other nations (Kerby et al., 2012). In the North Sea fishery, a mix of demersal fishing methods is used, varying in their impact on the seafloor. In the Greater North Sea mobile bottom trawling is estimated to have been deployed on 46.5% of the total area in 2015 by commercial vessels of the >12 m category (ICES, 2016). The four gear types (fishing métiers) used primarily in the North Sea fishery are otter trawl (OTB), beam trawl (TBB), dredge and demersal seine. Additionally, electrical trawling occurs in the German Bight but is of minor importance (ICES, 2020). They all belong to the category of active demersal fishing gears, which are operating in direct contact with the seafloor and consequently modify seafloor properties by ploughing and scarping, and cause disturbance of the upper surface sediments (Jones, 1992; Oberle et al., 2016). Resuspension of sediment is induced by hydrodynamic drag generated in the wake of the gear (O'Neill and Summerbell, 2011; Bradshaw et al., 2012; Martín et al., 2014; O'Neill and Ivanović, 2016), with the consequence that sediment is redistributed, whereby finer particles can be carried away by currents and heavier particles settle more quickly (Palanques et al., 2014; Oberle et al., 2015; Mengual et al., 2016). The amount and magnitude of impact on the seafloor is strongly dependent on several factors like: towing speed, gear type and its configuration (dimension, weight and different riggings), substrate and currents (Jones, 1992; Jennings et al., 1999), but natural sediment dynamics have to be considered as well (Oberle et al., 2017). The generation of trawl marks has been observed in all substrate types, but the depth of the trawl marks is a matter of debate. Penetration depths given in the literature for soft sediments, depending on used gear, range from the top centimeters (Løkkeborg, 2005) to 30 cm (Jones, 1992). Simply put, the effects can vary depending on the sediment type and are less in hard substrate like sand than in softer substrate like mud or silt. The fine-scale footprint of bottom trawling in the German EEZ of the North Sea for the four gear types mentioned above during the period of 2012–2016 is displayed in Fig. 1C. The footprint of bottom trawling was estimated for vessels >12 m in size by a satellite-based vessel monitoring system (VMS), linked to the corresponding logbook information (German fleet) or the European fleet register (international fleet), respectively (Hintzen et al., 2012). It is quantified as annual swept area ratio, which is the ratio between the cumulative area touched by trawls and the size of the respective grid cell (0.05◦*0.05◦). As expected the fishing pressure is highest near to the coast where also small vessels can operate and in a corridor of the northeastern continuation of the Elbe glacial valley outside the Natura 2000 area.

Beam trawl

Beam trawl is predominantly deployed in the shallower southern North Sea (ICES, 2018), whereby smaller vessels (Eurocutters) are operating in coastal areas for shrimp fishery and larger beam trawlers targeting mainly flatfish are predominant in the offshore areas (outside the 12 NM zone) (Van Hal et al., 2010). The net is held open horizontally by a rigid steel beam attached to a beam head (trawl shoes) at each end (Polet and Depestele, 2010). Depending on substrate type, different configurations of the ground rope are used to disturb the seabed surface by penetrating the upper centimeters of the sediment to flush target species (mainly deep burrowing flatfish species like sole) from the seabed into the net. Tickler chains, attached between the beam trawl shoes, are commonly used for soft or sandy grounds and alternatively the trawl is equipped with chain mats for rougher grounds with pebbles and boulders (Van Hal et al., 2010; Polet and Depestele, 2010). The weight (in air) of a complete beam trawl varies from several hundred kilograms for a shrimp trawl to up to 7 tons (and more) for the flatfish trawls equipped with tickler chains (Polet and Depestele, 2010). Generally, two trawls are towed by means of outriggers booms on each side of the vessel (TBB-twin/double-rig beam trawl). The highest pressures are exerted by the trawl heads, lesser by the tickler chains or chain mats, but these interact with the seafloor over a greater area (Polet and Depestele, 2010; Eigaard et al., 2015). The overall footprint is relative homogeneous in comparison to the otter-trawl footprint (Eigaard et al., 2015) (see below).

Demersal otter trawl

Demersal otter trawling is used in North Sea fishery to catch round fish species like cod, whiting and haddock or crustacea like Nephros that live close above the seabed (Polet et al., 1994). It is applied within the entire North Sea, but primary in the central part of the North Sea (Polet and Depestele, 2010). Horizontal opening of the cone-shape net is achieved by two otter boards (also called doors) that are connected to the vessel by warps and to the trawl net by sweeps (Buhl-Mortensen et al., 2013; Eigaard et al., 2015). These hydrofoils, designed to maintain firm contact with the bottom and spread the trawl mouth open, can have various designs and a weight of hundreds of kilograms (Coggan et al., 2001). The separation distance of the otter boards is around 60–120 m and only one otter trawl is deployed per ship (Van Hal et al., 2010). Depending on the substrate the gear is equipped with different types of ground rope (e.g. bobbin, roller, rockhopper) to ensure close contact with the bottom and prevent damage of the trawl net on rougher grounds. The heavy trawl doors have the most evident physical effect on the seafloor compared to other parts of the gear due to a higher penetration depth and sediment displacement (Eigaard et al., 2015). Depending on sediment type and door configuration (angle of attack and weight) they may generate more or less distinct berms and furrows which are deeper and more pronounced on soft than on firm substrates (Krost et al., 1990; Linnane et al., 2000). The furrow depth can vary between a few centimeters (Mayer et al., 1991) and more than 20 cm (Krost et al., 1990; Løkkeborg, 2005) having width of 0.2 m (Humborstad et al., 2004) up to 2 m (Caddy, 1973; Krost et al., 1990). Over the entire length the OTB gear penetrates not as deep into the sediment as the TBB (lesser seafloor impact), but the OTB affects much larger areas and the zone of disturbance shows higher heterogeneity (Eigaard et al., 2015).

3. Data and Method

Hydrographic survey

In this study we present the results of three cruises HE422 (May 2014), HE468 (July 2016) and HE471 (Sept. 2016). Operating platform was in each case the RV Heincke and the data were obtained with the ships own hull mounted Kongsberg Maritime EM710 multibeam echosounder. The MBES is maintained and calibrated by a service company on a yearly basis. The system is designed for shallow to medium water depths and operates between 70 and 100 kHz with an angular coverage up to 140◦. We used the single swath, high-density mode with 200 equidistant soundings per ping. The system was operated mostly in shallow mode with a minimum individual beam width of 1 × 2° (Table 1). Ping rate varied with operation mode and time synchronization between alternately triggered MBES and SBES. Vertical resolution of the system computes to 0.375 m and spatial resolution depends on water depth in the study areas (29–50 m) and grazing angles (0–60°). It varies between 0.5 and 3.5 m in across-track and 0.5–1.74 m in along-track direction, respectively (applying the formulas for MBES in Lurton, 2010). Swath distance related to ping rate and survey speed was about 0.8 m. The MBES data were recorded with the SIS (Seafloor Information System) software package of KONGSBERG compensated for ship motion (pitch, roll, heave and yaw) and corrected for sensor geometry, absorption, sound velocity variations at the transducers and in the water column. Variations in absorption and sound velocity were minor because due to the rough sea state (Table 1; wind speed) the water column was entirely mixed. As most MBES systems, the EM710 is optimized for bathymetric mapping and therefore its swath is subdivided into various transmit sectors (3 in the case of the EM710) to maximize range capability but also to suppress interference from multiples of strong bottom echoes. The sectors are transmitted sequentially within each ping, and use distinct gains, frequencies or waveforms. To avoid these real-time backscatter adjustments, we selected a fixed operating mode in the SIS software, to apply a constant pulse length; in addition, we turned off the sector tracking function to eliminate gain normalization; and we activated the penetration filter to equalize at least the frequencies of both outer sectors. Sound velocity profiles were obtained during the cruises using a Valeport MIDAS SVP probe and were continuously measured by a hull mounted sound probe near the transducer position. Overlap between the survey lines varies between 9 and 20% and was on average 15.6% (Table 1). Post-processing with the Qimera software of QPS includes (1) tide correction (EM2008 European Shelf, Oregon State University tidal model); (2) slant range correction by applying a measured sound velocity profile for each survey area; (3) data cleaning (via manual editing and CUBE uncertainty filtering). The resulting digital elevation models have a cell size of 1 m (Table 1). The revised bathymetric surface is then transferred into the Fledermaus Geocoder Toolbox (FMGT) software of QPS for slope correction during mosaicking and ARA analysis (see below) with the implemented Geocoder algorithm. The Geocoder software was originally developed at the Center for Coastal and Ocean Mapping (CCOM) at the University of New Hampshire (Fonseca and Calder, 2005; Fonseca and Mayer, 2007; Fonseca et al., 2009; Rzhanov et al., 2012). The FMGT Geocoder toolset processes acoustic backscatter data for mosaic (backscatter reflectivity map) creation and seafloor characterization.

In this study we present the results of three cruises HE422 (May 2014), HE468 (July 2016) and HE471 (Sept. 2016). Operating platform was in each case the RV Heincke and the data were obtained with the ships own hull mounted Kongsberg Maritime EM710 multibeam echosounder. The MBES is maintained and calibrated by a service company on a yearly basis.

The system is designed for shallow to medium water depths and operates between 70-100 kHz with an angular coverage up to 140°. We used the single swath, high-density mode with 200 equidistant soundings per ping. The system was operated mostly in shallow mode with a minimum individual beam width of 1 x 2° (Tab. 1). Ping rate varied with operation mode and time synchronization between alternately triggered MBES and SBES. Vertical resolution of the system computes to 0.375 m and spatial resolution depends on water depth in the study areas (29 to 50 m) and grazing angles (0-60°). It varies between 0.5-3.5 m in across-track and 0.5-1.74 m in along-track direction, respectively (applying the formulas for MBES in Lurton, 2010). Swath distance related to ping rate and survey speed was about 0.8 m. The MBES data were recorded with the SIS (Seafloor Information System) software package of KONGSBERG compensated for ship motion (pitch, roll, heave and yaw) and corrected for sensor geometry, absorption, sound velocity variations at the transducers and in the water column. Variations in absorption and sound velocity were minor because due to the rough sea state (Tab. 1; wind speed) the water column was entirely mixed. As most MBES systems, the EM710 is optimized for bathymetric mapping and therefore its swath is subdivided into various transmit sectors (3 in the case of the EM710) to maximize range capability but also to suppress interference from multiples of strong bottom echoes. The sectors are transmitted sequentially within each ping, and use distinct gains, frequencies or waveforms. To avoid these real-time backscatter adjustments, we selected a fixed operating mode in the SIS software, to apply a constant pulse length; in addition, we turned off the sector tracking function to eliminate gain normalization; and we activated the penetration filter to equalize at least the frequencies of both outer sectors. Sound velocity profiles were obtained during the cruises using a Valeport MIDAS SVP probe and were continuously measured by a hull mounted sound probe near the transducer position. Overlap between the survey lines varies between 9 and 20 % and was on average 15.6 % (Tab. 1). Post-processing with the Qimera software of QPS includes (1) tide correction (EM2008 European Shelf, Oregon State University tidal model); (2) slant range correction by applying a measured sound velocity profile for each survey area; (3) data cleaning (via manual editing and CUBE uncertainty filtering). The resulting digital elevation models have a cell size of 1 m (Tab. 1). The revised bathymetric surface is then transferred into the FMGT software of QPS for slope correction during mosaicking and ARA analysis (see below) with the implemented Geocoder algorithm. The Geocoder software was originally developed at the Center for Coastal and Ocean Mapping (CCOM) at the University of New Hampshire (Fonseca and Calder, 2005; Fonseca and Mayer, 2007; Fonseca et al. 2009; Rzhanov et al. 2012). The FMGT Geocoder toolset processes acoustic backscatter data for mosaic (backscatter reflectivity map) creation and seafloor characterization.

Backscatter strength

The beam time-series data, previously cleaned from artefacts in Qimera, has been processed with FMGT using standard work flow for calibrated Kongsberg Maritime .all-files. The latter very closely fulfill the criteria established by Schimel et al. (2018) concerning proper documentation of built-in backscatter corrections. The software uses the Geocoder algorithm introduced and described in Fonseca and Calder (2005). In the program, the backscatter values are reduced to a near-calibrated scale of scattering strength by applying a radiometric and geometric correction. Default settings were applied for angle varying gain adjustment, including the flat algorithm with a window size of consecutive 300 pings and adaptive normalization that uses a reference angle between 20° and 60° (Fonseca et al., 2009). The backscatter strength depends on several system parameters like frequency, pulse length and

beam width which have been kept constant during all cruises. The backscatter values are plotting in shades of grey whereby white and black symbolizes highest and lowest strength, respectively. The highest possible resolution for each mosaic was automatically calculated by FMGT and varies from 0.26 m to 0.43 m (Table 1).

Beam Pattern Analysis

An important step in backscatter and ARA processing is the radiometric correction. This is archived in FMGT by the use of the beam pattern correction tool that computes the theoretical backscatter curve based on granulometry of bottom samples and subtracts it from the measured backscatter to receive the sonar-related contribution of the seafloor return. For a detailed description of the beam pattern correction method in FMGT we refer to Santos et al. (2018). The beam pattern after its correction is shown in Fig. 2 for each NOAH study area, together with the angular response curve of the composite roughness model after (Jackson et al., 1986). This mathematical model generates an expected acoustic response curve as a function of grazing angle vs. returned backscatter strength. Prerequisite for a successful beam pattern determination is an almost flat seafloor patch with known homogeneous lithology. We used one sample for each survey within the respective NOAH areas. Although, the sonar-related contribution of the beam pattern should be constant for each survey, the sediment impact may change by area. This is probably because of the varying amount of shell fragments and bioturbation not considered by the Jackson model.

Angular Range Analysis

The Angular Range Analysis implemented in the Geocoder tool of FMGT is a method of seafloor characterization which compares the actual backscatter angular response (an intrinsic property of the seafloor) to expected acoustic response curves based on the Jackson model. Thirty consecutive acoustic pulses (parameter not modifiable) of each side of the swath are stacked into two distinct seafloor patches (port and starboard side) in FMGT to reduce the speckle noise, but this decreases the spatial resolution of the ARA maps. To discriminate the returned backscatter into components, the stacked response is divided into discrete angular ranges including the near range with incident angles from 0° to 25°, the far range from 25° to 55°, and the outer range from 55° to 85° (Fonseca et al., 2005; Fonseca and Mayer, 2007). In general, the backscatter is strongly angle-depending and consists of different components. A transmitted sound wave impinging on the water-sediment interface can be subdivided in its specular component that is reflected away from the receiver and the portion of the signal that is scattered by the interface relief and returned to the receiver (e.g., Lurton, 2010). Another portion of the signal penetrates the sediment and is scattered at heterogeneities in the subsurface (e.g., buried rocks, shell fragments, animals or gas bubbles). Furthermore, the volume backscatter depends on the grain size dominating in soft sediments and diminishing in coarse silt and very fine sand due to absorption (compilation of absorption coefficients in Lurton, 2010). At incidence angles close to vertical, the scatter is controlled by subhorizontal facets and at grazing incidence by the microscale roughness (Lurton, 2010). For the ARA several parameters are extracted from the backscatter angular response curve, including the average backscatter strength, slope, intercept and orthogonal distance. For a detailed description of the ARA-parameters refer to Fonseca et al. (2005) and Fonseca and Mayer (2007). In the process, the inversion of the model is done iteratively by adjusting the ARA parameters from the model to the observations constrained by the established inter-property relationships (Hamilton, 1974; Richardson and Briggs, 2004). The inversion of the

model generates estimates of the acoustic impedance, volume scatter, roughness and mean grain size of the insonified seafloor patch. The acoustic impedance is addressed by the index of impedance (the product of sediment bulk density and sound velocity ratio in g cm^{-3}). The volume scatter measured in dB includes that part of the transmitted energy that penetrates the sediment interface and is scattered back at matrix heterogeneities. The seafloor roughness is expressed in terms of rms (root mean square) heights in cm. The calculated grain size is indicated in the Krumbein (1938) phi (ϕ) scale.

Sediment sampling and grain size analysis

Bottom sediment sampling was conducted within the acoustically surveyed area by van Veen grab to calibrate MBES backscatter and cross-check the ARA results. In Fig. 2 we show only calibration results for one survey per study area, however, we ground-truthed all surveys per area. The deviation between ARA and sample analysis in phi (ϕ) units are shown in the respective ARA results map of each NOAH area. In average the deviation (square root) is very low, reaching 0.30, 0.26 and 0.06 phi for NOAH I, NOAH G and NOAH D, respectively. Samples in areas of different backscatter types were taken from the uppermost centimeter immediately after recovery of the grab. Particle size distribution was determined using laser granulometry (Sympatec Helos KF) in the laboratory at the University of Hamburg. Samples for bulk grain size were wet-sieved (2000 µm) prior to measurement to remove very coarse particles. Additionally, all carbonate particles and organic matter was removed. To ensure accuracy of measurements and absence of a long-term instrumental drift, an in-house grain-size standard was measured regularly. Using the classification of Folk (1954) the samples rank from very coarse silt in NOAH G to fine sand in NOAH I. Grain-size statistics are based on the graphical method (Folk and Ward, 1957) and were calculated using Gradistat (Blott and Pye, 2001). Results are expressed in phi units and plotted in Fig. 2.

Video tracks

For additional ground-truthing, video recordings of the seafloor were obtained within each NOAH study area during the HE422 cruise (see images in Fig. 2 and tracks in bathymetric maps). The dataset is used to determine the seafloor roughness and to visualize the prevailing habitat including faunal and floral colonization. The video system is self-constructed by the Helmholtz-Zentrum Geesthacht (Germany). It consists of a sledge equipped with a HD video system. The sledge dimension is 1.0 × 0.7 × 1.9 m (width, height, length). The video system (manufactured by C-Technics) is based on a HD-Camera, 2 LED-lamps for illumination, 2 He–Ne lasers for a reference distance on ground and is connected by an umbilical of 200 m length to a computer. The acquisition software allows real-time inspection as well as recording of the video signal superimposed with the actual GPS position of the ship. The sledge was towed behind the vessel with a speed of about 1 kn above ground.

Calculation of furrow density

To calculate the density of the furrows, we used the ArcGIS software from ESRI. We chose the mosaic as base map because all furrows appear in the mosaic but not in the bathymetry. An attempt to automatically discriminate the furrows from the background based on their grey values was not successful. Consequently, we manually digitised the furrows for each cruise data set. In a second step a buffer was calculated around the mapped polylines applying the average furrow width of 14 m measured in the mosaic. This processing step creates polygons representing the area occupied by the furrows. This procedure was only applied for NOAH I;

in NOAH G and D individual tracks were not distinguishable and the density was visually estimated.

4. Results

4.1 NOAH I

The area lies in the south-eastern part of the Dogger Bank within a water depth range of 29–33 m (Fig. 1). Video recordings display a seafloor covered by small ripples and shell fragments (Fig. 2). Analysis of seabed samples gave a grain size of fine sand with a significant percentage of embedded shell fragments. The sand is well-sorted and loosely packed supporting a high mobility of the grains.

4.1.1 Bathymetry

The seafloor topography is relatively smooth, dipping gently from south to north (Fig. 3A). NNW-SSE striking sinuous, subaqueous small dunes of 1–6 cm in height and wavelengths of 2–6 m (after the classification of Ashley et al., 1990) cover the seabed (see next section). Video observations indicate that the small dunes are superimposed by smaller ripples not being detectable at the resolution of the MBES bathymetric data (Table 1). These small variations (micro-scale roughness) are therefore not considered in the real slope corrections of the incidence signals and may cause fluctuations of the average backscatter (Roche et al., 2018) depending on the survey direction (Lurton et al., 2017). Abundant parallel pairs of furrows with a width of 6–9 m and a separation distance of 20–23 m is visible on the bathymetric map (Fig. 3B2, C2 and D2). They are irregularly distributed and crossing in places. For HE422, their depth is about 5–7 cm and for HE468 it is only 4 cm. We term these furrows Type 1.

4.1.2 Backscatter

In general, the backscatter in this study area is relatively homogeneous, without any visible differences in intensities between the cruises (Fig. 3B1, C1a and D1). However, the abundant occurrence of pairs of parallel tracks of higher backscatter (lighter grey tones) is typical for the entire study area. The tracks have a width and a separation distance of 6.5–8 m and 19.5–23.5 m, respectively. They do not exhibit a preferred orientation. Many of the paired tracks are crossing and in places, the intersecting tracks show different backscatter strength. A comparison of the tracks in the backscatter with those in the bathymetry of cruise HE422 reveals that the two are congruent and correspond to Type 1. However, during cruise HE468, many of the backscatter paired tracks of Type 1 have no morphological expression in the bathymetry. The dunes seen in the bathymetry are also visible in the backscatter (Fig. 3C1b). In HE422 two single tracks of ca. 65 and 90 m width of low backscatter occur without any bathymetric expression, but clear indications in the ARA results. Notable is the fact that only at nadir they show higher backscatter compared to the background. This striking pattern was also observed in NOAH G (see below) where it is associated with another type of furrows, we term Type 2 (see below).

4.1.3 Angular range analysis

The ARA sediment type classification and grain size computation is in close accordance with the seabed sampling results. In the study area fine sand dominates with values of 2.63 phi (ARA) and 2.2 phi (samples) (Figs. 2 and 4A). There is a slight difference between the port and starboard sides which we attribute to instrumentation parameters of the Kongsberg EM710

system. Unfortunately, the system transmits in 3 sectors that cannot be operated mono-frequent. This may affect the reproducibility of the ARA results under certain circumstances. There is also a slight difference in the ARA results of HE468 and HE422a compared to HE422b. Although HE422a and HE422b were surveyed on two subsequent days, the rougher sea state during HE422a (Table 1; wind speed 11 m s^{-1} instead of 8 m s^{-1}) may have affected the measurements. However, the deviation in mean grain size is only about 0.2 phi, which is still in the fine sand range. Some of the paired furrows of Type 1 seen in the mosaic and bathymetry are clearly displayed in the ARA image, but appear only as single lines because of the low ARA resolution (see section 3.4). There are two trends: HE422 shows coarser grain sizes (lower phi values) in the furrows compared to the background values, whereas the opposite, namely finer grain sizes (higher phi values) in the furrows is seen during HE468. Some of the furrows are also visible in the index of impedance map showing lower densities (1.45 g cm^{-3}) for HE468 and higher (1.75 g cm^{-3}) for HE422 (Fig. 4B). The average background value is about 1.6 g cm^{-3}. In the micro topography map (rms roughness), the furrows are characterized by low roughness with values around 2.5 cm (Fig. 4C). The mean for the entire area is 3 cm, which coincides with the small dunes observed in the bathymetry. In general, the volume scattering strength exhibits high values in the eastern part of the study area (Fig. 4D). The furrows in HE422 are indicated by low volume scatter in contrast to furrows in HE468 which show high volume scatter. The two wide furrows seen in the backscatter image have larger grain size, higher impedance as well as lower RMS roughness and volume scatter compared to the surrounding seafloor (arrows in Fig. 4A). Their absolute width cannot be deduced from the ARA inversion because of the low spatial resolution (Table 1). They have no bathymetric expression and are probably Type 2 furrows.

4.1.4 Furrow density

To calculate the density of the observed Type 1 furrows in the backscatter and the affected area, an average width of the marks of 7 m was assumed (Fig. 5). The spatial extent of the multibeam survey HE422 was ca. 28.76 km^2 of which 2.30 km^2 were swept by beam trawls. HE468 covered an area of 10.44 km^2 wherefrom 2.10 km^2 were trawled. These results account for 8 % and 20 % of the seafloor impacted by fishing activity in May 2014 and July 2016, respectively. The lower swept ratio corresponds with the data compiled from the logbook information or European fleet register (average 2–5) and the fact that the area belongs to a Natura 2000 site (Fig. 1C).

4.1.5 Furrow conservation potential

For a comparison study of the long-term conservation potential of the seafloor disturbance by the groundgear, we compared the backscatter mosaics of two surveys covering the same seafloor domain in NOAH I. They were carried out in May (HE422) and September 2014 (HE432). The results document that some of the furrows left by the fishing gear persist at least over the observation period of 4 months (Fig. 6).

4.2 NOAH G

The area lies on the inner shelf ca. 120 km westward of the Island Sylt (Fig. 1). Analysis of seabed samples shows that the sediment is very fine to muddy sand without embedded shell fragments (Fig. 2). Video recordings display a hummocky seafloor relief created by burrowing-epifauna. The higher fine fraction content compared to NOAH I enhances the cohesion between the grains and makes the sediment stiffer.

4.2.1 Bathymetry

The seabed topography smoothly dips northeastward spanning a water depth range of 44.2–48.8 m (Fig. 7A). The area is characterized by NE-SW striking sinuous, subaqueous small dunes with wavelengths of 3–5 m, heights of 3–10 cm (after classification of Ashley et al., 1990) (Fig. 7D). Additionally, HE468 shows many parallel small furrows with a width of ca. 2 m and a depth of ca. 5 cm. Some exhibit a berm on one side (Fig. 7B2, E and F). The paired furrows mainly strike NNW-SSE with separation distances of 110–120 m (Fig. 7B2 and E). In contrast, the adjoining HE422 data do not show any similar structure. We term these furrows as Type 2. Type 1 furrows were morphological only identified in HE468 data. They have a width of ca. 10 m, a separation distance of 22–25 m and a depth of ca. 6 cm.

4.2.2 Backscatter

In general, the backscatter is relatively homogeneous. Unfortunately, the nadir domain of the MBES data is overamplified and shows along-track (W-E) artefacts (Fig. 7B1 and C1; N). The HE468 data are dominated by parallel lineations between the furrows, light grey nadir and dark grey at grazing angle (Fig. 7B1). They are associated with the Type 2 furrows. In some zones they are densely spaced, whereas in between they occur only occasionally. Similar features are absent in the HE422 data, where paired tracks of high backscatter are common, analogous to NOAH I. The tracks belong to Type 1 and have widths of ca. 10 m with a separation distance of about 20 m (Fig. 7C1). They display a random distribution. However, despite their high abundance in the backscatter data, they exhibit no topographic expression in the bathymetry. HE468 backscatter data display these tracks only in places, whereby some have a clear expression in the bathymetry.

4.2.3 Angular range analysis

The ARA-based sediment type classification and grain size computation resembles the seabed sampling results. The area is dominated by very fine to muddy sand with a computed mean grain size of 3.46 phi (Figs. 2 and 8A). In general, sediments become slightly muddier from west to east by 0.1 phi. Whereas HE422 sediment type distribution is relatively homogeneous, HE468 displays a distinct pattern of coarse-grained tracks mainly orientated NNW-SSE. They correspond with the zones of backscatter lineations described above and thus lie between the Type 2 furrows seen in the bathymetry (Fig. 7B2 and E). These tracks are characterized by a high impedance, low rms roughness and low volume scattering (Fig. 8B–D). In contrast, HE422 data exhibit a uniform rms roughness of ca. 2.5 cm (mean). Higher values, representing a rougher micro-topography like seen in HE468, are absent. Additionally, the volume scattering strength in HE422 data is generally low (0.9 dB) and gradually increases from east to west, which is in accordance with an increase in grain size and acoustic impedance. Tracks of higher volume scatter like in HE468 do not occur (Fig. 8D).

4.2.4 Furrow density

A determination of the Type 1 furrow number was not feasible because of their very high abundance which made it impossible to trace individual furrows (Fig. 7C1). A tentative estimation of the seafloor impacted by fishing activity for NOAH G yields considerably higher magnitudes of 80–90 % as compared to NOAH I. The Type 2 furrows and their associated zones occupy ca. 50–60 % of the HE468 area (Fig. 7B1). The swept area ratio map of Fig. 1C clarify these differences showing significant higher values for NOAH G compared to NOAH I.

4.3 NOAH D

The area lies on the inner shelf ca. 40 km off the coastline (Fig. 1). Analysis of seabed samples shows a grain size of very fine sand with imbedded shell fragments. The latter are less abundant than at NOAH I and the sediment is also stiffer (Fig. 2). Video recordings display small ripples covering the sea floor.

4.3.1 Bathymetry

In general, seabed topography is relatively smooth (Fig. 9). The water depth ranges between 33 and 37.5 m, gently dipping towards NE. On the bathymetric map scattered parallel pairs of furrows with a width of 7–9 m and a separation distance of 16–18 m are visible that can be classified as Type 1 (Fig. 9 B2 and C2). The furrows are randomly distributed and compared to area NOAH I they are deeper, reaching values of 6–10 cm. Some areas, like a small hill topped by a wreck, show significant trawling impact. Here, the accumulation of furrows surrounding the hill is very high, individual furrows are hardly distinguishable and they are deeper than 10 cm (Fig. 9C2).

4.3.2 Backscatter

The backscatter is relatively homogeneous and only the furrows appearing in the bathymetry are visible as dark lines (Fig. 9B1 and C1). This implies, contrary to NOAH I, that the scatter intensity of the furrows is lower than that of the background sediment.

4.3.3 Angular range analysis

As for NOAH I and G, the ARA sediment type classification and grain size computation for NOAH D is in close accordance with the seabed sampling results (Figs. 2 and 10A). Dominant sediment type is very fine sand with a computed average grain size of 3.23 phi. In contrast to NOAH I, the computed phi, index of impedance and roughness do not display any significant anomalies related to the furrows seen in the backscatter and bathymetry (Fig. 10A–D), although the ARA resolution (smaller patch size) is higher compared to the other study areas (Table 1). The roughness is on average about 2.3 cm and uniformly developed in the entire area (Fig. 10C). Only in places the furrows are indicated by a low volume scatter (Fig. 10D, arrows).

4.3.4 Furrow density

Like for NOAH G, a determination of the Type 1 furrow density was impossible because of their very high density seen in the mosaic (Fig. 9B1 and C1). A tentative estimation of the seafloor impacted by fishing activity for NOAH D yields considerable magnitudes of 80–90 %. The swept ratio map shows that NOAH D lies between NOAH I and G, tending more to higher values.

5. Discussion

5.1 Origin of furrows

The nature and intensity of the impact (footprint) on the physical environment are specific to each gear type owing to their varying catching principles (Polet and Depestele, 2010; Lucchetti and Sala, 2012). In general, we observed 2 types of long, linear furrows in the three NOAH study areas. Both types appear as paired, almost parallel topographic features. However, in some of our datasets the tracks can only be recognized in the backscatter (see further

discussion). The first and more common Type 1 occurs in all study areas (Figs. 3, 7 and 9). The associated paired furrows have widths of 6–9 m and a depth of 2–10 cm with a separation distance of 16–23 m (Table 2). The second Type 2 was only found in NOAH G during the July cruise HE468 in 2016 (Fig. 7B1 and B2) and probably also in the North of NOAH I (HE422) (Fig. 4A, arrows). The Type 2 furrows are much narrower, but have a larger separation distance of 110–120 m. Characteristic for Type 2 is a zone of high and low backscatter lineations between the furrows. We interpret both types of paired seabed footprints as evidence of demersal trawling activity. They are traces of fishing gear that left their imprint on the seafloor. In the North Sea two main types of fishing gear are used: TBB and OTB, respectively (see section 2). Beam trawlers exhibit a configuration that correlates well with our Type 1 hydroacoustic properties (see also section 2). The physical impact of the beam trawl on the seabed is compaction of the sediments and its lateral and vertical displacement over the entire width of the gear (e.g. Depestele et al., 2015). Small-scale bedforms like ripples or biogenic structures will be levelled out under the weight of the gear (Polet and Depestele, 2010). As reported by Rowden et al. (1998) the physical properties of the sediment may be affected by the burrowing and feeding activity of macrobenthos community that lowers bulk density and rigidity. These changes in sediment fabric will likely alter the hydroacoustic behavior of the upper seafloor and therefore be displayed in the ARA maps. Closing of the burrows inside the sediment due to ploughing and elimination of micro roughness at the sediment-water interface by trawling will change the surface and volume backscatter behavior of the signal. The dimension and separation distance of the observed tracks agree also with electrical pulse fishing. In this métier, however, only the two electrode arrays have ground contact, towed at each side of the fishing vessel, by means of outriggers (each 12 m in width and consisting of 12–14 cables). They are scratching the seabed, but cannot produce centimeter deep furrows. Additionally, the pulse trawl effort in the German Bight is very low (ICES, 2020). Furrow Type 2 in NOAH G can be correlated with single otter trawl tracks, clearly expressed in the bathymetry (Fig. 7B2, E and F). Their separation distance of 110–120 m in the hydroacoustic data correlates with typical gear dimensions (see section 2). The ground rope, the trawl net and the sweeps that affect most of the swept area, mainly skim off surface sediments and create only faint marks (Krost et al., 1990; Buhl-Mortensen et al., 2013; O'Neill and Ivanović, 2016), but flatten sedimentary features or biogenic structures (Schwinghamer et al., 1996; Smith et al., 2000). These zones between the otter boards, where the net and the weighted ground rope touches the seafloor displays stripes of varying backscatter strength (Fig. 7B1). The two otter board themselves have the greatest impact in terms of sediment displacement. They leave narrow furrows (door marks) in the seabed that are only seen in the bathymetry (Fig. 7B2, E and F). Core profiles taken inside and outside the trawl marks by Mayer et al. (1991) indicate that no ploughing and sediment mixing occurs in the area between the door marks. In the case of type 2 furrows, we rule out electrical trawling as the cause of the stripes in the backscatter, because the electrode arrays are only 12 m wide (ICES, 2020).

5.2 Hydroacoustic properties of furrows

Our results document that the habitus of the observed bottom tracks depends on intrinsic factors like the type of seabed substrate, the amount of embedded shell fragments and burrowing fauna. Possible extrinsic factors are the type and weight of fishing gear, the towing speed and hydrodynamic regime. For both fishing methods, TBB and OTB, we compiled a model that demonstrates the physical impact of bottom trawling on different seabed substrates and the respective backscatter contributions of the observed acoustic signatures

(Figs. 11 and 12). The displayed angular response curves delineate the average backscatter strength of 30 consecutive pings (one ARA patch) within the bottom trawl tracks and the adjacent undisturbed seabed.

Regarding the visibility of the fishing gear traces there is a clear difference between the morphological expression and the returned signal strength. Comparing the backscatter images with the prevailing bathymetry reveals that furrows found in the bathymetry in most cases are expressed by seabed returns with different scattering intensities than the background. However, not all paired linear backscatter anomalies have expressions in the bathymetry. One possible explanation for this discrepancy is the infill of older furrows by sediments, in general finer material as discussed later. During the survey of the northern part of NOAH I (HE422) we apparently recorded a situation when the impact of fishing activity was relatively fresh. Here, the furrows exhibit high backscatter strength correlating with a coarser seabed (lower phi values) and higher impedances (Fig. 3B1, 3C1a, 4 A and 4 B, Table 2). The grounding gear penetrates the subbottom and easily suspends the predominant loosely packed fine sand (Fig. 2). From the resultant sediment plume the coarser fraction then resettles in situ after gear passage and the finer is blown away (Fig. 11, case A). The modeled mean current of 16.6 m s 1 for NOAH I (Table 1) is high enough to transport fine sand in suspension. The winnowing of the finer fraction may result in an accumulation of coarse-grained shell fragments at the bottom of the tracks generating a sort of shell pavement (Lindeboom and De Groot, 1998). All factors result in an increase of sediment density in the furrows in relation to the surrounding seafloor as seen in the computed impedance (Fig. 4B, Table 2). The abundance of shell fragments in NOAH I is also depicted by an overall higher volume backscatter strength compared to NOAH D and G (Figs. 2, 4D, 8D and 10D). Shell fragments at the seafloor and within the subsurface return more emitted energy (Lurton, 2010). In contrast to the northern part, the ARA results in the southern part of NOAH I (HE468) document the filling of the TBB tracks by finer particles (very fine sand; Fig. 4A and Table 2), especially where the tracks lack a topographic signature. Additionally, the index of impedance points to a less dense infill (lower values; Fig. 4B and Table 2). It is suggested that finer grains mobilized by current and wave energy accumulate over time in the furrows (Fig. 11, case B). Although it is expected that the finer material in the tracks lowers the backscatter strength by enhancing the specular contribution due the flattening the micro-relief, the overall backscatter strength is still higher compared to the background (Fig. 3D1 and Table 2). We explain this observation by an increase of the volume scatter contribution to the backscatter (Figs. 4D and 11, case B). Accordingly, the acoustic energy penetrates the infill of the furrows and is scattered at its coarse-grained base. Penetration of the acoustic signal in sandy substrate is 9 cm at a frequency of 100 kHz (Huff, 2008) used in this study. From the mosaic alone, the high backscatter strength in HE468 (Fig. 3D1) would have erroneously point to coarser infill material. This result documents the added value of using ARA in the interpretation. In the northern part of NOAH G surveyed in July 2016 (HE468) we found tracks of otter boards that left a different pattern on the seabed. These boards also create furrows, but they are much narrower compared to the beam trawls. They are clearly seen in the bathymetry and in places in the backscatter image (Fig. 7B2 and E), but not in the ARA results (Fig. 8A–D). The latter data, however, show the imprint of the fishing net towed between the otter boards and touching the seabed with its ground rope (Fig. 12). In the ARA results, these zones are characterized by lower phi values, higher impedance, lower roughness and lower volume scatter compared to the background (Fig. 8A–D). In the backscatter, this contact area is displayed as a zone of parallel stripes of low intensity between the otter board tracks (Fig.

7B1). However, at nadir location they exhibit high backscatter. These observations can be best explained by a trawling-induced flattening of the seafloor or the change of the (micro) roughness orientation due to the ground rope components of the gear (Fig. 12B). By touching the ground, the weight-armed ground robe destroys the micro-scale roughness and suspends the finer fraction that is carried away by the bottom current. The decrease of the roughness along the trawling tracks is clearly documented by the rms roughness (Fig. 8C). In general, a smoothed seafloor will contribute to a distinct enhancement of the coherent reflection energy (Lurton, 2010). At near vertical incidence a maximum of the reflection energy is returned from the flattened surface causing the observed nadir high backscatter (Fig. 7B1 and 12B, NR). With decreasing grazing angle, the flattened seabed reflects most of the energy away from the MBES (specular scatter, e.g. Lurton and Lamarche, 2015). Only a small portion is scattered back to the MBES which lowers the backscatter strength along the narrow parallel stripes where the gear grounded (Fig. 12B, FR and OR). Additionally, the loss of the finer fraction (here silt, Fig. 2) due to sediment mobilization by the groundgear leads to a bottom substrate coarsening expressed by lower phi-values (Fig. 8A). The resulting increase in sand fraction induces a higher energy absorption within the sediment, or a reduction in energy that finally penetrates the seabed which also contributes to a lower volume backscatter along the tracks (Fig. 8D). Before and after otter trawl experiments (sediment cores) carried out by Palanques et al. (2001) detect only minor changes in sediment grain size inside the tracks one day after trawl. Schwinghamer et al. (1998) came to a similar conclusion that otter trawling is not influencing the grain size (detected by RoxAnn). These findings are in agreement with our inference of a flattened seabed. Mengual et al. (2016) substantiate our observation of substrate coarsening after the passage of a trawl in areas of strong currents, which they attribute to winnowing and lateral dispersal of the resuspended fine fraction. The situation in the southern part of NOAH G (HE422) is comparable to that at NOAH I (HE468). The tracks are of Type 1 are generally less visible in the bathymetry, but clearly indicated by high backscatter strength (Figs. 3 and 7C1 and 7C2). Only a few furrows are seen in the morphology, particularly in the north of NOAH G (HE468). The very dense pattern of beam trawling tracks (Type 1) is clearly displayed in the backscatter (Fig. 7C1). Like in NOAH I (HE468), we suggest that most of the tracks are refilled with sediment and therefore show no morphologic expression in the southern sector of NOAH G (HE422). Unfortunately, because the prevailing very high track density exceeding the resolution of the ARA patches (Table 1), no differences in the ARA parameter could be discriminated in NOAH G (HE422) (Fig. 7C1 and 8A-D, see also section 3). NOAH D is dominated by fine sand with shell fragments and covered by small centimeter-sized ripples (directed roughness). The latter are below the lateral MBES resolution of ca. 80 cm (Fig. 2). The area is characterized by a very high density of paired furrows clearly expressed in the bathymetry and backscatter (Fig. 9B1, B2, C1 and C2). In contrast to NOAH I and G, the tracks are marked by low backscatter. We conclude that in the case of NOAH D the gear of the TBB penetrates the seabed and flattens the micro-relief in the tracks (Fig. 11, case C). Unfortunately, the ARA results display no variability, except that the volume scatter has low values in tracks oriented in along-patch direction, perpendicular to the sailing line (arrows in Fig. 10D). Hence the volume scatter contribution to the backscatter strength must be very low inside the tracks (Fig. 11, case C). Part of the sediment is mobilized into the water column and is transported away by the bottom current. The stronger hydrodynamic regime (mean current velocity 38.8 m-1; Table 1) may also prevent the refilling of tracks over extended time leading to good preservation in the bathymetry. By losing their roughness the tracks show lower backscatter compared to the background. This mechanism would be comparable to the OTB scratches in NOAH G (HE468).

5.3. Fishing stress

Fishing pressure on a large scale can be estimated by VMS data in combination with the m´etier information of the vessel from the logbook data and is expressed in “impacted surface in a period of time” (Rijnsdorp et al., 2011; Hintzen et al., 2012; Eigaard et al., 2017). In general, fishing activities are spread over the entire North Sea area, but show spatial and temporal variability, resulting in a patchiness of fishing effort within the North Sea (Lindeboom and De Groot, 1998; Jennings et al., 1999). Distribution and intensity of fishing effort depend on several factors like dispersal of the target species (Poos and Rijnsdorp, 2007; Polet and Depestele, 2010), “skippers choice” (Rijnsdorp et al., 2011), fishing quotas (Rijnsdorp et al., 2008) as well as other factors like oil price (Van Hal et al., 2010). Additionally, the existence of wind parks or marine protection areas limits the accessibility for the fishing industry (Fig. 1C). Moreover, the used fishing gears also show varying distribution patterns across the North Sea (ICES, 2017). Consequently, there can be areas under high fishing pressure while others are rarely fished (Fig. 1C). Our data reveals a high interannual variation in the density of trawl marks in the study areas (Table 2). Furthermore, we observed a predominant use of beam trawls within all studied NOAH areas, whereas otter trawlers were deployed only in a part of NOAH G during the summer season (HE468; Table 2) and possibly in NOAH I. The MBES data clearly document the heavy physical impact (area and depth of seabed penetration) of beam trawling on the seabed in NOAH D (September; Table 2) and NOAH G (May, HE422; Table 2). The observed tracks are randomly distributed and the entire seafloor is virtually ploughed over several centimeters deep (Fig. 7C1, 9B1, 9B2, 9C1 and 9C2). This intense surface and subsurface alteration may significantly affect the living conditions of the benthic community. If the habitat can recover to normal conditions or whether this is the normal state remains questionable and needs further investigation. Our study shows that the long-term conservation potential of the seafloor disturbance by the groundgear is at least 4 months (see section 3). In addition, we do not know the age of the tracks at the time of investigation. During our surveys we observed no fishing activity in the study areas. Therefore, the actual conservation potential could be much longer. Studies document that seafloor alterations and trawl marks can have varying longevity depending on the substrate (because penetration is lower in sandy sediments due to the high mechanical resistance of the sediment) (DeAlteris et al., 1999) and natural remediating factors like bioturbation, wave action and currents (Jones, 1992; Polet and Depestele, 2010; Palanques et al., 2001). Another factor which was not further examined in this study is the impact of bacteria. They are extremely abundant in marine sediments, exude mucus or extracellular polysaccharides that can “glue” together the particles in sediment at the grain-to grain contact points (Murray and Jumars, 2002). This may locally form quasi-rigid viscoelastic structures that stabilise the furrows by changing the bulk physical (frame) and acoustical properties that differ from the surrounding materials.

6. Conclusions

Our hydroacoustic investigation documents the potential of an MBES to detect the physical impact of demersal fishing activity on different seafloor habitats in the SE North Sea. Its use allows the extensive mapping of shallow water areas and it has a clear advantage over conventional sidescan acquisition that only registers the seafloor backscatter. With the combined use of the amplitude and depth information the user is able to additionally extract the angle-dependent signal parts of the seabed returns. The ARA derivatives of the insonified area include roughness, impedance, volume scatter and medium grain size permit more differentiated and reliable predictions of the physical stress on the seafloor habitat. It provides

information about the sediment type, micro-scale relief and the subbottom nature. These are all intrinsic factors that influence the effects of bottom trawling.

MBES remote sensing is a valuable tool to directly study the impact of ground-touching gear and complement other observation methods like VMS. In the future, investigations have to be extended to coarser and mixed seafloor habitats to evaluate the reliability of the applied methods. Furthermore, the long-term impact of ground fishing should be monitored and compared with natural seafloor disturbances induced by currents and waves. As a general recommendation, the MBES has to be carefully calibrated and it is mandatory to use the same instrument and processing software to obtain verifiable results.

Author statement

Thomas Lüdmann: conceptualization, methodology, writing (original draft), writing (review and editing), supervision, visualization, Yannick Saitz: writing (review and editing), investigation, validation, visualization, Jan Metzing: investigation, validation, visualization, Kay- Christian Emeis: writing (review and editing), project administration, funding acquisition.

Declaration of competing interest

The authors declare that they have no known competing financial interests or personal relationships that could have appeared to influence the work reported in this paper.

Acknowledgements

We thank the captain and the crew of the RV Heincke for support during the cruises. The study was funded by the University of Hamburg and the Federal Ministry of Education and Research in the framework of the NOAH project (03F0669F and 03F0742C). We also thank Editor Gary Fones and four anonymous reviewers for providing constructive comments that contributed to improve this manuscript.

7. References

Alevizos, E., Snellen, M., Simons, D., Siemes, K., Greinert, J., 2018. Multi-angle backscatter classification and sub-bottom profiling for improved seafloor characterization. Mar. Geophys. Res. 39, 289–306. https://doi.org/10.1007/s11001-017-9325-4.

Anderson, J.T., Van Holliday, D., Kloser, R., Reid, D.G., Simard, Y., 2008. Acoustic seabed classification: current practice and future directions. ICES J. Mar. Sci. 65, 1004–1011.

Ashley, G.M., 1990. Classification of large-scale subaqueous bedforms: a new look at an old problem-SEPM bedforms and bedding structures. J. Sediment. Petrol. 60, 160–172.

Benn, A.R., Weaver, P.P., Billet, D.S., Van Den Hove, S., Murdock, A.P., Doneghan, G.B., Le Bas, T., 2010. Human activities on the deep seafloor in the North East Atlantic: an assessment of spatial extent. PloS One 5, e12730.

Blott, S.J., Pye, K., 2001. GRADISTAT: a grain size distribution and statistics package for the analysis of unconsolidated sediments. Earth Surf. Process. Landforms 26 (11), 1237–1248.

Bradshaw, C., Tjensvoll, I., Skold, M., Allan, I.J., Molvaer, J., Magnusson, J., Naes, K., Nilsson, H.C., 2012. Bottom trawling resuspends sediment and releases bioavailable contaminants in a polluted fjord. Environ. Pol. 170, 232–241.

Brown, C.J., Blondel, P., 2009. Developments in the application of multibeam sonar backscatter for seafloor habitat mapping. Appl. Acoust. 70, 1242–1247.

Brown, C.J., Smith, S.J., Lawton, P., Anderson, J.T., 2011. Benthic habitat mapping: a review of progress towards improved understanding of the spatial ecology of the seafloor using acoustic techniques. Estuar. Coast Shelf Sci. 92 (3), 502–520. https:// doi.org/10.1016/j.ecss.2011.02.007.

Buhl-Mortensen, L., Aglen, A., Breen, M., Buhl-Mortensen, P., Ervik, A., Husa, V., Lokkeborg, S., Rottingen, I., Stockhausen, H.H., 2013. Impacts of fisheries and aquaculture on sediments and benthic fauna: suggestions for new management approaches. Fisken Havet 2, 69.

Caddy, J.F., 1973. Underwater observations on tracks of dredges and trawls and some effects of dredging on a scallop ground. J. Fisheries Board of Canada 30, 173–180.

Cameron, T.D.J., Crosby, A., Balson, P.S., Jeffery, D.H., Lott, G.K., Bulat, J., Harrison, D.J., 1992. United Kingdom offshore regional report: the geology of the southern North Sea. HMSO for the Brit. Geol. Sur., p. 152

Coggan, R.A., Smith, C.J., Atkinson, R.J.A., Papadopoulou, K.N., Stevenson, T.D.I., Moore, P.G., Tuck, I.D., 2001. Comparison of Rapid Methodologies for Quantifying Environmental Impacts of Otter Trawls. DG XIV Study Project No. 98/017.

DeAlteris, J., Skrobe, L., Lipsky, C., 1999. The significance of seabed disturbance by mobile fishing gear relative to natural processes: a case study in Narragansett Bay, Rhode Island. Am. Fish. Soc. Symp. 22, 224–237.

Depestele, J., Ivanovic, A., Degrendele, K., Esmaeili, M., Polet, H., Roche, M., Summerbell, K., Teal, L.R., Vanelslander, B., O'Neill, F.G., 2015. Measuring and assessing the physical impact of beam trawling. ICES J. Mar. Sci. 73 (Suppl. 1), i15–i26.

Diesing, M., Ware, S., Foster-Smith, R., Stewart, H., Long, D., Vanstaen, K., Forster, R., Morando, A., 2009. Understanding the marine environment – seabed habitat investigations of the Dogger Bank offshore draft SAC. Joint Nature Conservation Committee, Peterborough. JNCC Rep. No. 429, 5 (Appendices).

Eastwood, P.D., Mills, C.M., Aldridge, J.N., Houghton, C.A., Rogers, S.I., 2007. Human activities in UK offshore waters: an assessment of direct, physical pressure on the seabed. ICES J. Mar. Sci. 64 (3), 453–463.

Eigaard, O.R., Bastardie, F., Breen, M., Dinesen, G.E., Hintzen, N.T., Laffargue, P., Polet, H., et al., 2015. Estimating seabed pressure from demersal trawls, seines, and dredges based on gear design and dimensions. ICES J. Mar. Sci. 73, i27–i43.

Eigaard, O.R., Bastardie, F., Hintzen, N.T., Buhl-Mortensen, L., Buhl-Mortensen, P., Catarino, R., Gerritsen, H.D., 2017. The footprint of bottom trawling in European waters: distribution, intensity, and seabed integrity. ICES J. Mar. Sci. 74 (3), 847–865.

Folk, R.L., 1954. The distinction between grain size and mineral composition in sedimentary-rock nomenclature. J. Geol. 62 (4), 344–359.

Folk, R.L., Ward, W.C., 1957. Brazos River bar [Texas]; a study in the significance of grain size parameters. J. Sediment. Res. 27, 3–26.

Fonseca, L., Calder, B., 2005. Geocoder: an efficient backscatter map constructor. Proceedings of the U.S. Hydrographic Conference 2005, San Diego.

Fonseca, L., Mayer, L.A., Kraft, B., 2005. Seafloor Characterization through the Application of AVO Analysis to Multibeam Sonar data. Center of Coastal and Ocean Mapping. Paper 340. http://scholars.unh.edu/ccom/340.

Fonseca, L., Mayer, L.A., 2007. Remote estimation of surficial seafloor properties through the application angular range analysis to multibeam sonar data. Mar. Geophys. Res. 28, 119–126.

Fonseca, L., Brown, C., Calder, B., Mayer, L., Rzhanov, Y., 2009. Angular range analysis of acoustic themes from Stanton Banks Ireland: a link between visual interpretation and multibeam echosounder angular signatures. Appl. Acoust. 70, 1298–1304.

Freitas, R., Sampalo, L., Oliveira, J., Rodrigues, A.M., Quintino, V., 2006. Validation of soft bottom benthic habitats identified by single-beam acoustics. Mar. Pollut. Bull. 53, 72–79.

Hamilton, E., 1974. Prediction of deep-sea sediment properties: state-of-the-art. In: Inderbitzen, A.L. (Ed.), Deep-sea Sediments Physical and Mechanical Properties. Plenum Press, New York, pp. 1–43.

Hintzen, N.T., Bastardie, F., Beare, D., Piet, G.J., Ulrich, C., Deporte, N., Egekvist, J., Degel, H., 2012. VMStools: open-source software for the processing, analysis and visualisation of fisheries logbook and VMS data. Fish. Res. 115, 31–43.

Holler, P., Markert, E., Bartholom¨a, A., Capperucci, R., Hass, H.C., Kr¨oncke, I., Mielck, F., Reimers, H.C., 2016. Tools to evaluate seafloor integrity: comparison of multi-device acoustic seafloor classifications for benthic macrofauna-driven patterns in the German Bight, southern North Sea. Geo Mar. Lett. 37 (2), 93–109.

Huff, L.C., 2008. Acoustic remote sensing as a tool for habitat mapping in Alaska waters.

Mar. Habitat Mapp. Technol. Alsk 10, 29–45.

Hughes-Clarke, J.E., Mayer, L.A., Wells, D.E., 1996. Shallow-water imaging multibeam sonars: a new tool for investigating seafloor processes in the coastal zone and on the continental shelf. Mar. Geophys. Res. 18, 607–629.

Humborstad, O.B., Nottestad, L., Rapp, H.T., 2004. RoxAnn bottom classification system, sidescan sonar and video-sledge: spatial resolution and their use in assessing trawling impacts. ICES J. Mar. Sci. 61 (1), 53–56.

ICES, 2007. Acoustic seabed classification of marine physical and biological landscapes. ICES Coop. Res. Rep. 286, 183.

ICES, 2016. Interim Report of the Working Group on Spatial Fisheries Data (WGSFD), 17-20 May 2016, Brest, France, vol. 18. ICES CM 2016/SSGEPI, p. 244.

ICES, 2017. EU Request on Indicators of the Pressure and Impact of Bottom-ContactingFishing Gear on the Seabed, and of Trade-Offs in the Catch and the Value of landings. ICES Special Request Advicesr.2017.13. ICES, Copenhagen. http://ices.dk/sites/pub /Publication%20Reports/Advice/2017/Special_requests/eu.2017.13.pdf. (Accessed 14 May 2017).

ICES, 2018. Report of the working group on the assessment of demersal stocks in the North Sea and skagerrak (WGNSSK), 24 april–3 may 2018, ostend, Belgium. ICES CM 2018/ACOM ICES. 2020. ICES working group on electrical trawling (WGELECTRA). ICES Sci. Rep. 2 (37), 108. https://doi.org/10.17895/ices.pub.6006.

Jackson, D.R., Winebrenner, D.P., Ishimaru, A., 1986. Application of the composite roughness model to high-frequency bottom backscatter. J. Acoust. Soc. Am. 79, 1410–1422.

Jennings, S., Alvsvåg, J., Cotter, A.J.R., Ehrich, S., Greenstreet, S.P.R., Jarre-Teichmann, A., Mergardt, N., Rijnsdorp, A.D., Smedstad, O., 1999. Fishing effects in northeast Atlantic shelf seas: patterns in fishing effort, diversity and community structure. III. International trawling effort in the North Sea: an analysis of spatial and temporal trends. Fish. Res. 40, 125–134.

Jennings, S., Kaiser, M.J., 1998. The effects of fishing on marine ecosystems. In: Advances in Marine Biology, vol. 34. Academic Press, pp. 201–352.

Jones, J.B., 1992. Environmental impact of trawling on the seabed: a review. N. Z. J. Mar. Freshw. Res. 26 (1), 59–67.

Kaiser, M.J., Collie, J.S., Hall, S.J., Jennings, S., Poiner, I.R., 2002. Modification of marine habitats by trawling activities: prognosis and solutions. Fish Fish. 3 (2), 114–136.

Kerby, T.K., Cheung, W.W., Engelhard, G.H., 2012. The United Kingdom's role in North Sea demersal fisheries: a hundred year perspective. Rev. Fish Biol. Fish. 22 (3), 621–634.

Krost, P., Bernhard, M., Werner, F., Hukriede, W., 1990. Otter trawl tracks in Kiel Bay (Western Baltic) mapped by side-scan sonar. Meeresforschung/Rep. Mar. Res. 32 (4), 344–353.

Krumbein, W.C., 1938. Size frequency distribution of sediments and the normal phi curve. J. Sediment. Petrol. 7, 3–17.

Lindeboom, H.J., De Groot, S.J., 1998. IMPACT-II: the Effects of Different Types of Fisheries on the North Sea and Irish Sea Benthic Ecosystems, p. 404.

Linnane, A., Ball, B., Munday, B., van Marlen, B., Bergman, M., Fonteyne, R., 2000. "A Review of Potential Techniques to Reduce the Environmental Impact of Demersal Trawls", Irish Fisheries Investigations No. 7. Marine Institute, pp. 1–39.

Lokkeborg, S., 2005. Impacts of trawling and scallop dredging on benthic habitats and communities. FAO Fisheries Technical Paper 472, 58.

Lucchetti, A., Sala, A., 2012. Impact and performance of Mediterranean fishing gear by side-scan sonar technology. Can. J. Fish. Aquat. Sci. 69, 1806–1816.
Lurton, X., Lamarche, G., 2015. Backscatter Measurements by Seafloor-mapping Sonars. Guidelines and Recommendations. A Collective Report by Members of the GeoHab Backscatter Working Group. May), 1-200.
Lurton, X., 2010. An introduction to underwater acoustics. Principles and Applications, second ed. Springer, Berlin, Germany, p. 680.
Lurton, X., Eleftherakis, D., Augustin, J.-M., 2017. Analysis of seafloor backscatter strength dependence on the survey azimuth using multibeam echosounder data. Mar. Geophys. Res. https://doi.org/10.1007/s11001-017-9318-3.
Martín, J., Puig, P., Palanques, A., Rib´o, M., 2014. Trawling-induced daily sediment resuspension in the flank of a Mediterranean submarine canyon. Deep Sea Res. Part II Top. Stud. Oceanogr. 104, 174–183.
Mayer, L.M., Schick, D.F., Findlay, R.H., Rice, D.L., 1991. Effects of commercial dragging on sedimentary organic matter. Mar. Environ. Res. 31, 249–261.
Mayer, L.A., 2006. Frontiers in seafloor mapping and visualization. Mar. Geophys. Res. 27, 7–17.
Mengual, B., Cayocca, F., Le Hir, P., Draye, R., Laffargue, P., Vincent, B., Garlan, T., 2016. Influence of bottom trawling on sediment resuspension in the 'Grande-Vasi`ere'area (Bay of Biscay, France). Ocean Dynam. 66, 1181–1207.
Morris, H.E., Hamilton, E.L., Bucker, H.P., Bachman, R.T., 1978. Interaction of Sound with the Ocean Bottom: a Three-Year Summary. Naval Ocean Systems Center, San Diego, CA, p. 242. Tech. Rep.
Murray, J.L.S., Jumars, P.A., 2002. Clonal fitness of bacteria predicted by analog modeling. BioSci 52, 343–355.
Nafe, J.E., Drake, C.L., 1964. Physical properties of marine sediments. In: Hill, M.N. (Ed.), The Sea 3. John Wiley, New York, pp. 794–814.
NOAH, 2020. Tidal Residual and Intertidal Mudflat Model (TRIM) with Shear Stress and Ripples. https://coastmap.hzg.de/coastmap/modeldata/MODEL_ANALYSIS_TOOL.
Oberle, F.K., Swarzenski, P.W., Reddy, C.M., Nelson, R.K., Baasch, B., Hanebuth, T.J., 2015. Deciphering the lithological consequences of bottom trawling to sedimentary habitats on the shelf. J. Mar. Syst. 159, 120–131.
Oberle, F.K., Storlazzi, C.D., Hanebuth, T.J., 2016. What a drag: quantifying the global impact of chronic bottom trawling on continental shelf sediment. J. Mar. Syst. 159, 109–119.
Oberle, F.K., Puig, P., Martín, J., 2017. Fishing activities. In: Micallef, A., Krastel, S., Savini, A. (Eds.), Submarine Geomorphology. Springer, Cham, pp. 503–534.
O'Neill, F.G., Ivanović, A., 2016. The physical impact of towed demersal fishing gears on soft sediments. ICES J. Mar. Sci. 73, i5–i14.
O'Neill, F.G., Summerbell, K., 2011. The mobilisation of sediment by demersal otter trawls. Mar. Pollut. Bull. 62 (5), 1088–1097.
Otto, L., Zimmerman, J.T.F., Furne, K., Mork, M., Saetre, R., Becker, G., 1990. Review of the physical oceanography of the North Sea. Neth. J. Sea Res. 26, 161–238.
Palanques, A., Guill´en, J., Puig, P., 2001. Impact of bottom trawling on water turbidity and muddy sediment of an unfished continental shelf. Limnol. Oceanogr. 46, 1100–1110.
Palanques, A., Puig, P., Guill´en, J., Demestre, M., Martín, J., 2014. Effects of bottom trawling on the Ebro continental shelf sedimentary system (NW Mediterranean). Continent. Shelf Res. 72, 83–98.
Polet, H., Blom, W., Thiele, W., 1994. An inventory of vessels and gear types engaged in the Belgian, Dutch and German bottom trawling. In: de Groot, S.J., Lindeboom, H.J. (Eds.), Environmental Impact of Bottom Gears on Benthic Fauna in Relation to Natural Resources Management and Protection of the North Sea. Netherlands Institute for Sea Research, Den Burg, Texel, pp. 7–20.
Polet, H., Depestele, J., 2010. Impact Assessment of the Effects of a Selected Range of Fishing Gears in the North Sea. ILVO, p. 120.
Poos, J.J., Rijnsdorp, A.D., 2007. The dynamics of small-scale patchiness of plaice and sole as reflected in the catch rates of the Dutch beam trawl fleet and its implications for the fleet dynamics. J. Sea Res. 58, 100–112.

Rice, J., Arvanitidis, C., Borja, A., Frid, C., Hiddink, J., Krause, J., Lorance, S., Ragnarsson, A., Skold, M., Trabucco, B., 2010. Marine Strategy framework directive – task group 6 report seafloor integrity. EUR 24334 EN 73.

Rice, J., Arvanitidis, C., Borja, A., Frid, C., Hiddink, J.G., Krause, J., Lorance, P., Ragnarsson, A., Skold, M., Trabucco, B., Enserink, L., Norkko, A., 2012. Indicators for sea-floor integrity under the European marine Strategy framework directive. Ecol. Indicat. 12 (1), 174–184.

Richardson, M.D., Briggs, K.B., 2004. Empirical predictions of seafloor properties based on remotely measured sediment impedance. In: Porter, M.B., Siderius, M. (Eds.), High-frequency Ocean Acoustic Conference. AIP Press, Melville, pp. 12–21.

Rijnsdorp, A.D., Poos, J.J., Quirijns, F.J., HilleRisLambers, R., De Wilde, J.W., Den Heijer, W.M., 2008. The arms race between Fishers. J. Sea Res. 60 (1–2), 126–138.

Rijnsdorp, A.D., Poos, J.J., Quirijns, F.J., 2011. Spatial dimension and exploitation dynamics of local fishing grounds by Fishers targeting several flatfish species. Can. J. Fish. Aquat. Sci. 68 (6), 1064–1076.

Rijnsdorp, A.D., Eigaard, O.R., Kenny, A., Hiddink, J.G., Hamon, K., Piet, G.J., Sala, A., Nielsen, J.R., Polet, H., Laffargue, P., Zengin, M., Gregersen, O., 2017. Assessing and Mitigating of Bottom Trawling. Final BENTHIS Project Report (Benthic Ecosystem Fisheries Impact Study), p. 28.

Roche, M., Degrendele, K., Vrignaud, C., Loyer, S., Le Bas, T., Augustin, J.M., Lurton, X., 2018. Control of the repeatability of high frequency multibeam echosounder backscatter by using natural reference areas. Mar. Geophys. Res. 39, 89–104.

Rowden, A.A., Jago, C.F., Jones, S.E., 1998. Influence of benthic macrofauna on the geotechnical and geophysical properties of surficial sediment, North Sea. Continent. Shelf Res. 18 (11), 1347–1363.

Rzhanov, Y., Fonseca, L., Mayer, L., 2012. Construction of seafloor thematic maps from multibeam acoustic backscatter angular response data. Comput. Geosci. 41, 181–187.

Santos, R., Rodrigues, A., Quartau, R., 2018. Acoustic remote characterization of seabed sediments using the Angular Range Analysis technique: the inlet channel of Tagus River estuary (Portugal). Mar. Geol. 400, 60–75.

Schimel, A.C.G., Beaudoin, J., Parnum, I.B., Le Bas, T., Schmidt, V., Keith, G., Ierodiaconou, D., 2018. Multibeam sonar backscatter data processing. Mar. Geophys. Res. 39, 121–137. https://doi.org/10.1007/s11001-018-9341-z.

Schwinghamer, P., Gordon Jr., D.C., Rowell, T.W., Prena, J., McKeown, D.L., Sonnichsen, G., Guign´e, J.Y., 1998. Effects of experimental otter trawling on surficial sediment properties of a sandy-bottom ecosystem on the Grand Banks of Newfoundland. Conserv. Biol. 12 (6), 1215–1222.

Schwinghamer, P., Guigne, J.Y., Siu, W.C., 1996. Quantifying the impact of trawling on benthic habitat structure using high resolution acoustics and chaos theory. Can. J. Fish. Aquat. Sci. 53 (2), 288–296.

Smith, C.J., Papadopoulou, K.N., Diliberto, S., 2000. Impact of otter trawling on an eastern Mediterranean commercial trawl fishing ground. ICES J. Mar. Sci. 57, 1340–1351.

Snellen, M., Eleftherakis, D., Amiri-Simkooei, A., Koomans, R.L., Simons, D.G., 2013. An inter-comparison of sediment classification methods based on multi-beam echosounder backscatter and sediment natural radioactivity data. J. Acoust. Soc. Am. 134, 959–970. https://doi.org/10.1121/1.4812858.

Stride, A.H., 1959. On the origin of the Dogger Bank in the North Sea. Geol. Mag. 96, 33–44.

Van Hal, R., Teal, L.R., Asjes, J., Jak, R.G., Scheidat, M., Craeymeersch, J.A.M., Bemmelen, R.S.A., Quirijns, F.J., Van Polanen-Petel, T., Deerenberg, C.M., 2010. Data availability for the fisheries impact assessment of the FIMPAS project. IMARES Wageningen C052/10, 119.

Van Moorsel, G.W.N.M., 2011. Species and Habitats of the International Dogger Bank. Ecosub, Doorn, p. 74.

Von Haugwitz, W., Wong, H.K., 1988. The Dogger Bank: seismic stratigraphy and Holocene sedimentation. — Mitt. Geol.-Palaeont. Inst. Univ. Hamb. 65, 409–422.

Watling, L., Norse, E.A., 1998. Disturbance of the seabed by mobile fishing gear: a comparison to forest clearcutting. Conserv. Biol. 12 (6), 1180–1197.

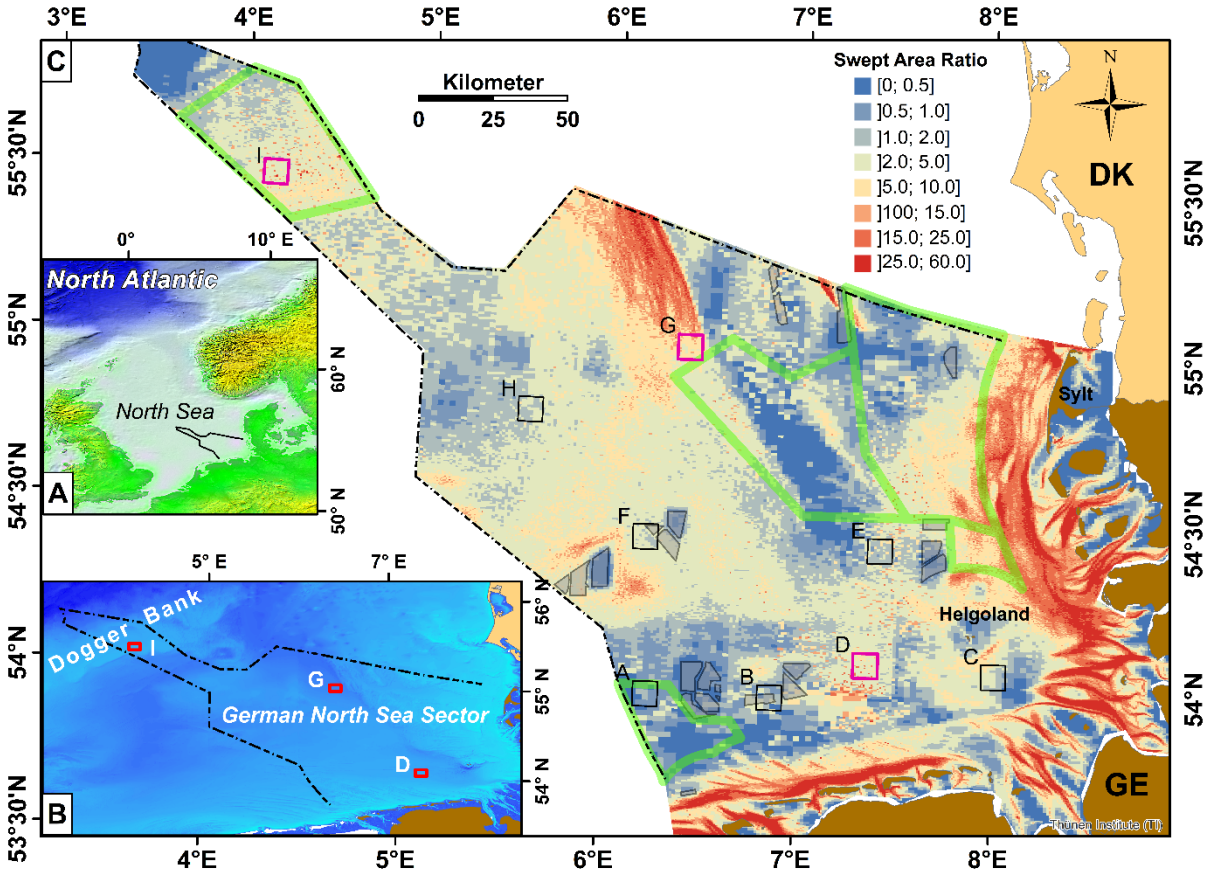

Fig. 1. (A) Regional map of the North Sea. Indicated is the German sector. (B) Map of the study area in the German North Sea sector (black dot-dashed line). Red box: NOAH areas discussed in this study. Bathymetry (http://www.emodnet-bathymet ry.eu). (C) Map of the swept area ratio averaged over the years 2012–2016 (http s://www.noah-project.de/habitatatlas/ind ex.php.de). It is based on VMS and logbook data and represents the ratio between the cumulative area touched by trawls and the size of the respective grid cell (0.05◦*0.05◦). Four major gear groups were considered including otter trawls, demersal seines, beam trawls and dredges (Hintzen et al., 2012). Black box: NOAH research areas A-I; red box: study area; green box: Natura 2000 area; grey box: wind park. DK: Denmark; GE: Germany.

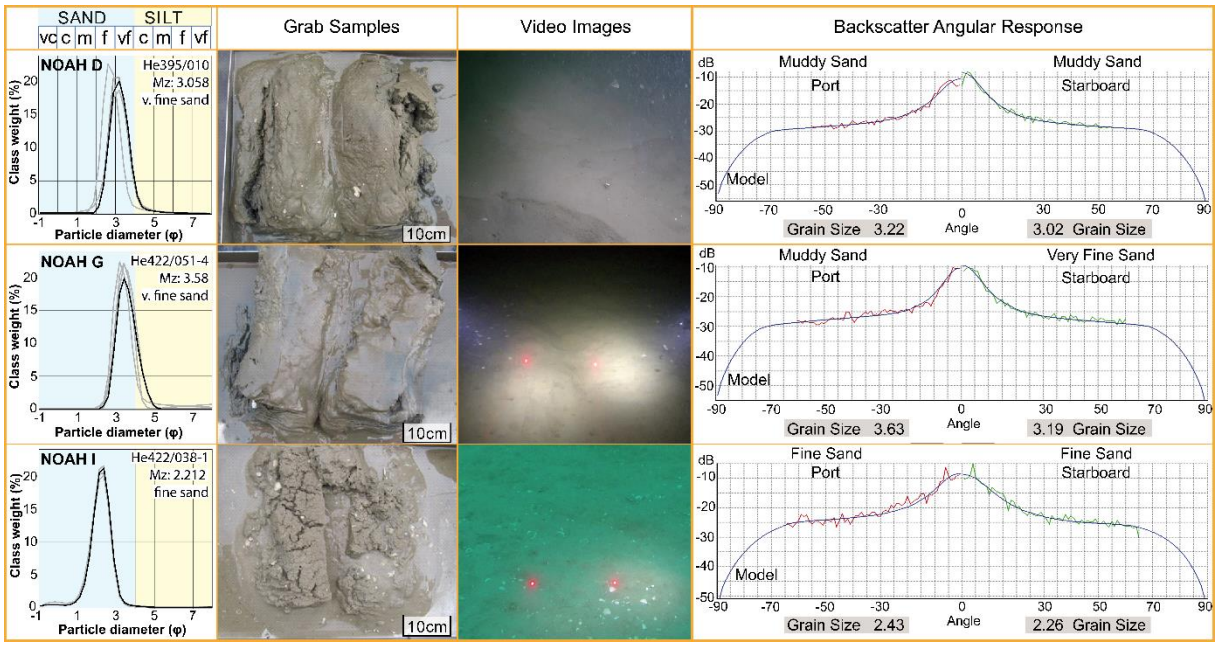

Fig. 2. Combined presentation of the grain size distribution in the three study areas, grab samples of prevailing seabed substrate, images of the seafloor (distance of red laser spots 12 cm) and MBES backscatter angular response after beam pattern correction (red and green line) at the ground-truth bottom sample stations (see location Figs. 3A, 7A and 9A). In addition, the angular response curve of the Jackson's model is shown (blue line) as well as the ARA computed mean grain size (phi) for port and starboard side. Black and grey curve indicate mean grain size at ground-truth bottom sample station and all other stations in the particular NOAH areas, respectively. Mz: mean grain diameter.

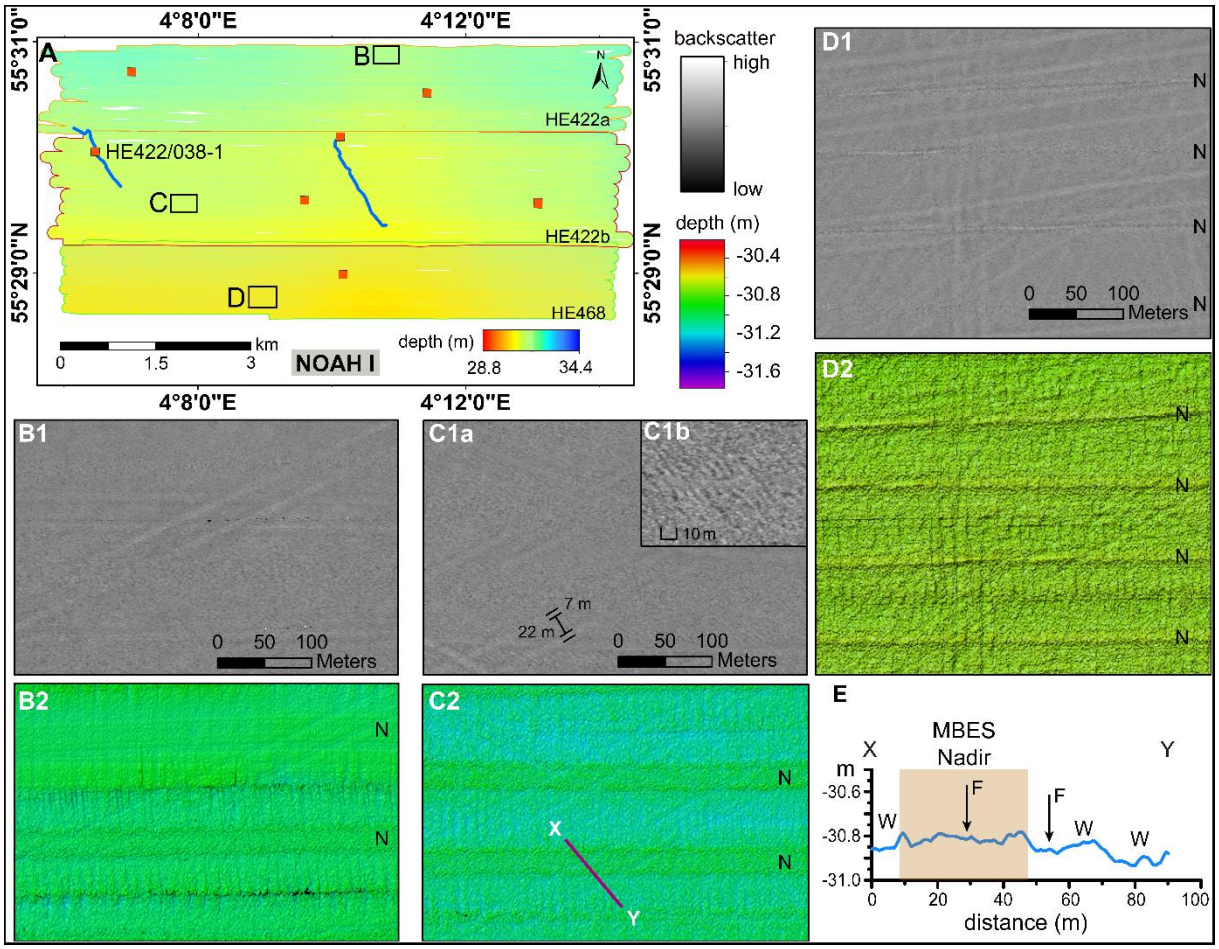

Fig. 3. A) Multibeam bathymetry of NOAH I (see location Fig. 1) with outline box of enlargements: backscatter (B1, C1a, C1b, D1) and bathymetry (B2, C2, D2). C1b) backscatter example (HE422b) of NNW-SSE striking sinuous sediment dunes. E) Topographic profile (see location in C2). F: furrow; N: MBES Nadir; W: wobble.

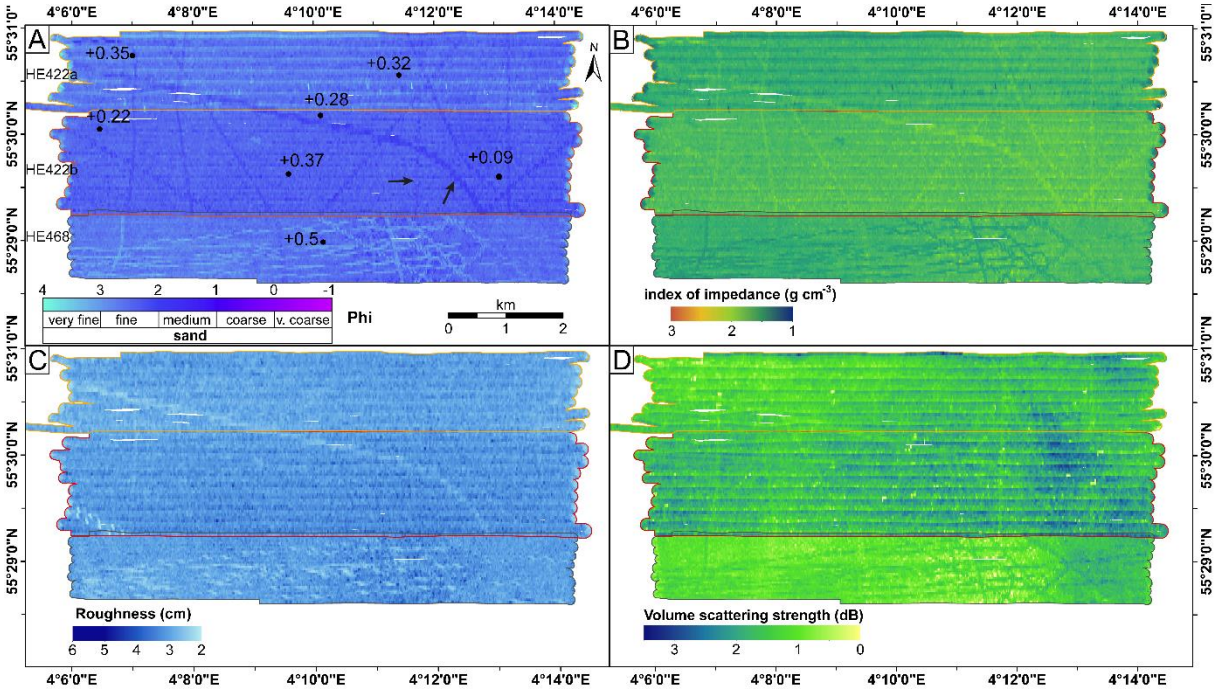

Fig. 4. NOAH I ARA-analysis including grain size (A), index of impedance (B), rms roughness (C) and volume scattering strength (D). Obvious are the tracks of the fishing gear. In HE422 the tracks are characterized by coarser material whereas HE468 points to finer. The latter tracks are older and refilled by finer particles. In contrast the other tracks are probably relatively fresh. The infill of the tracks is also accompanied by a decrease in impedance. The fresh tracks in HE422 display also a lower roughness and volume scattering caused by seabed flattening and compaction due to the heavy gear. Black arrows: see text for explanation. Black dots indicate sample location. Numbers reveal delta phi (mean grain size) between samples and ARA results.

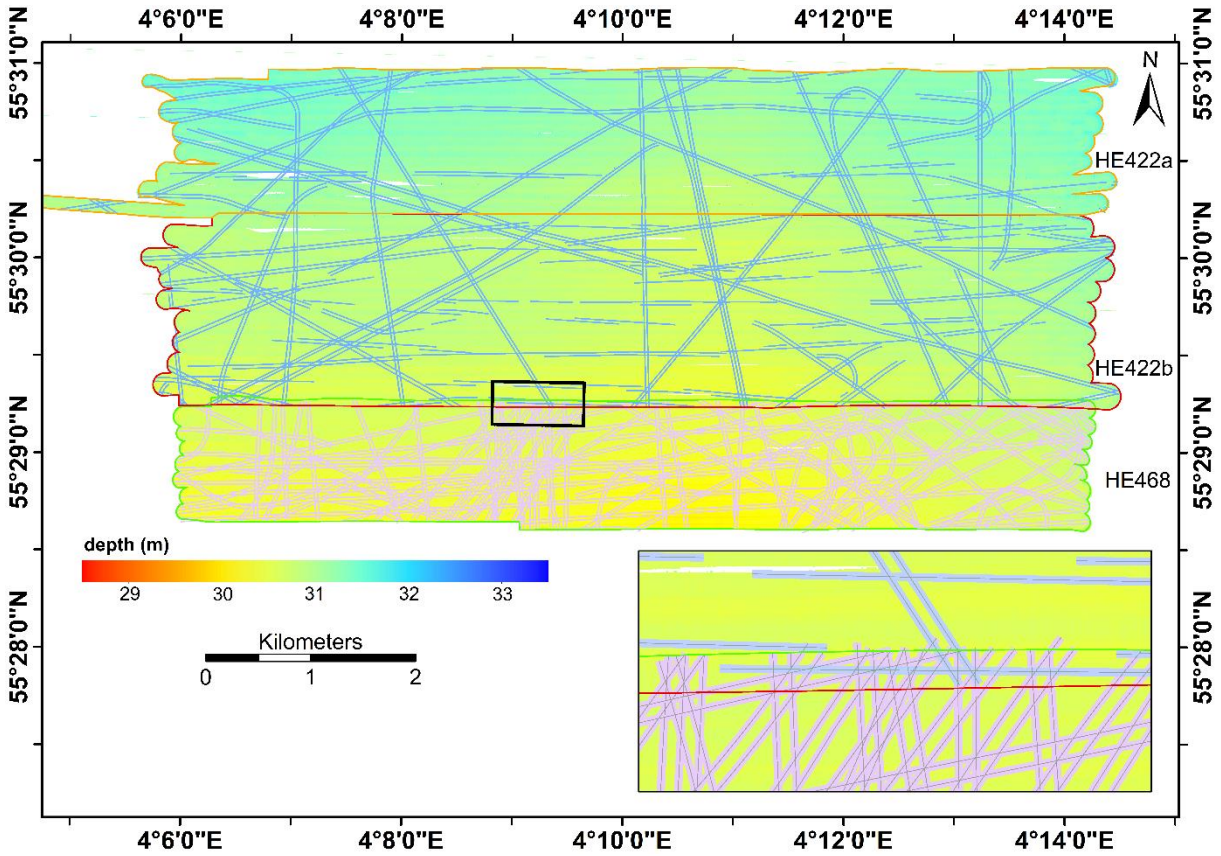

Fig. 5. Distribution of beam trawl tracks in NOAH I. See the difference in fishing activity between cruises HE422 and HE468 representing spring and summer season, respectively.

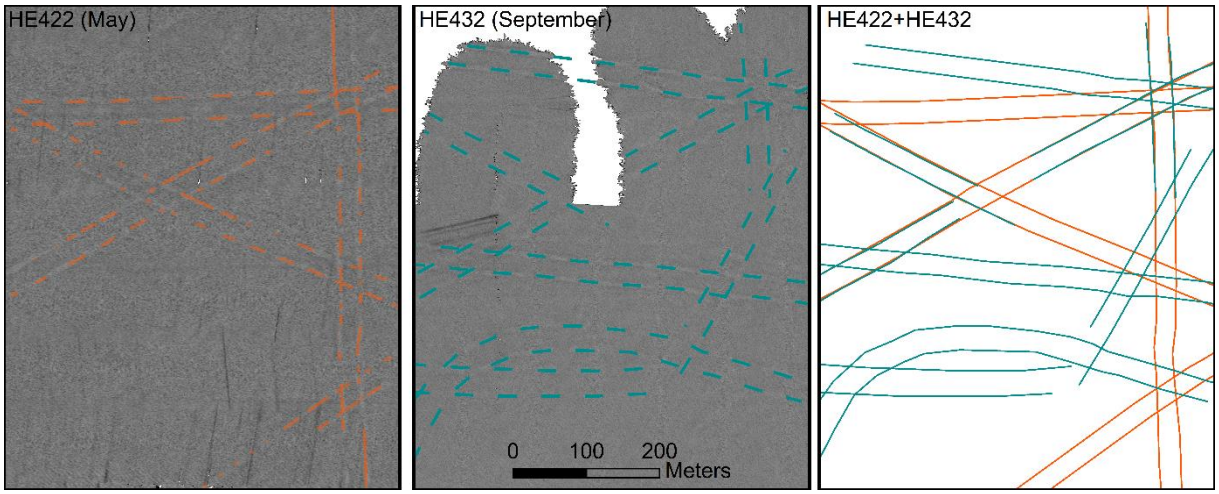

Fig. 6. Backscatter maps of HE422 and HE432 from the same location in NOAH I. The combined map overlays the marked trawling tracks of May and September 2014. It demonstrates that some of the tracks observed in May still existed after 4 months.

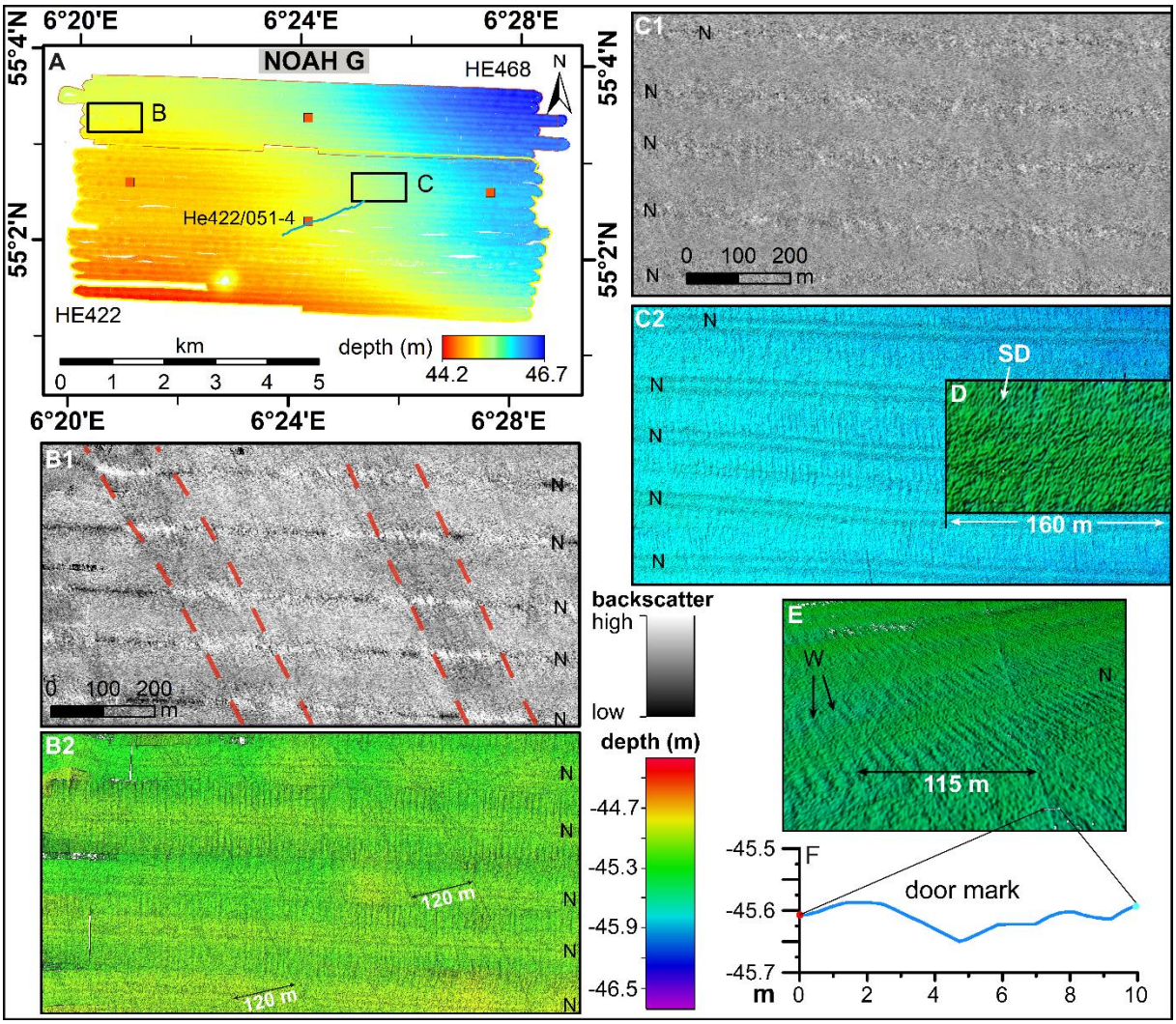

Fig. 7. Multibeam bathymetry of NOAH G (see location Fig. 1) with outline box of enlargements: backscatter (B1, C1) and bathymetry (B2, C2). Red dashed line: zone between Type 2 furrows showing stripes of backscatter anomalies. D) Enlarged bathymetry showing NE-SW striking sinuous dunes, characteristic for both survey areas. E) 3D view of bathymetry in HE468 with Type 2 furrows. F) Topographic cross section over furrow. N: MBES nadir; SD: sediment dune, W: wobbeling.

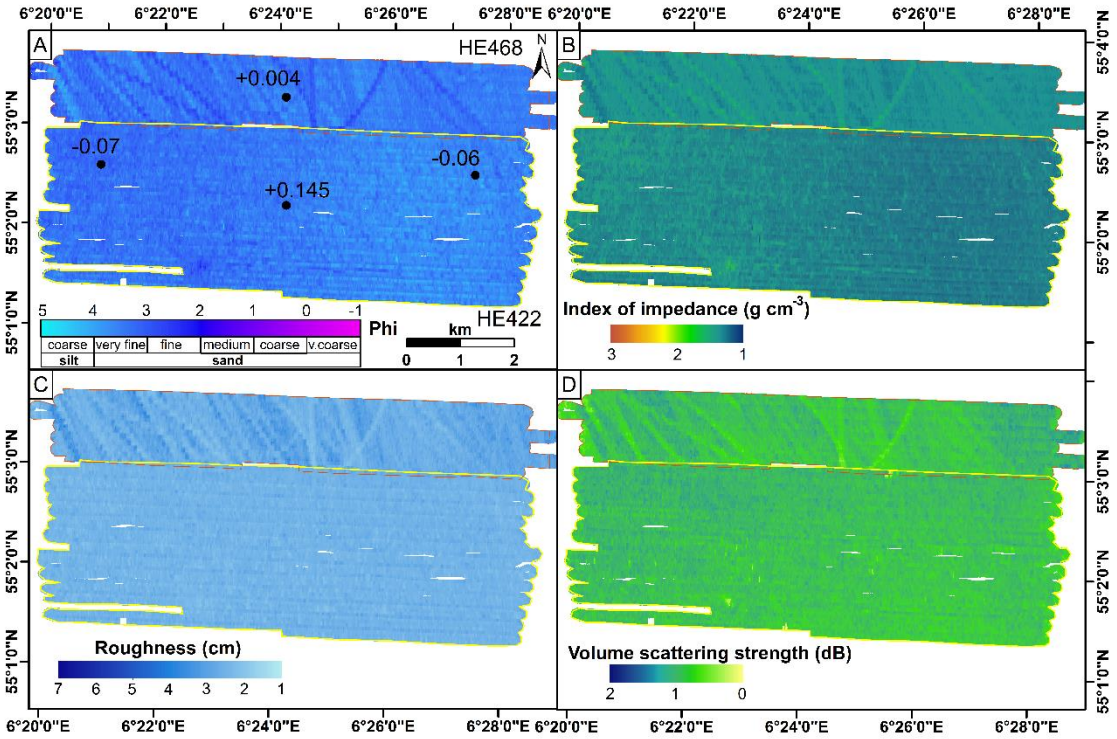

Fig. 8. NOAH G ARA-analysis including grain size (A), index of impedance (B), rms roughness (C) and volume scattering strength (D). Obvious are the discrepancies between HE468 and HE422. The ARA pattern seen in HE468 are typical for otter board trawling (Type 2 furrows). HE422 does not show any anomalies, here only beam trawling (Type 1 furrows) occurred (see Fig. 7; C1 and C2). Unfortunately, the very high track density in HE422 is below the resolution of the calculated ARA patches. Black dots indicate sample location. Numbers reveal delta phi (mean grain size) between samples and ARA results.

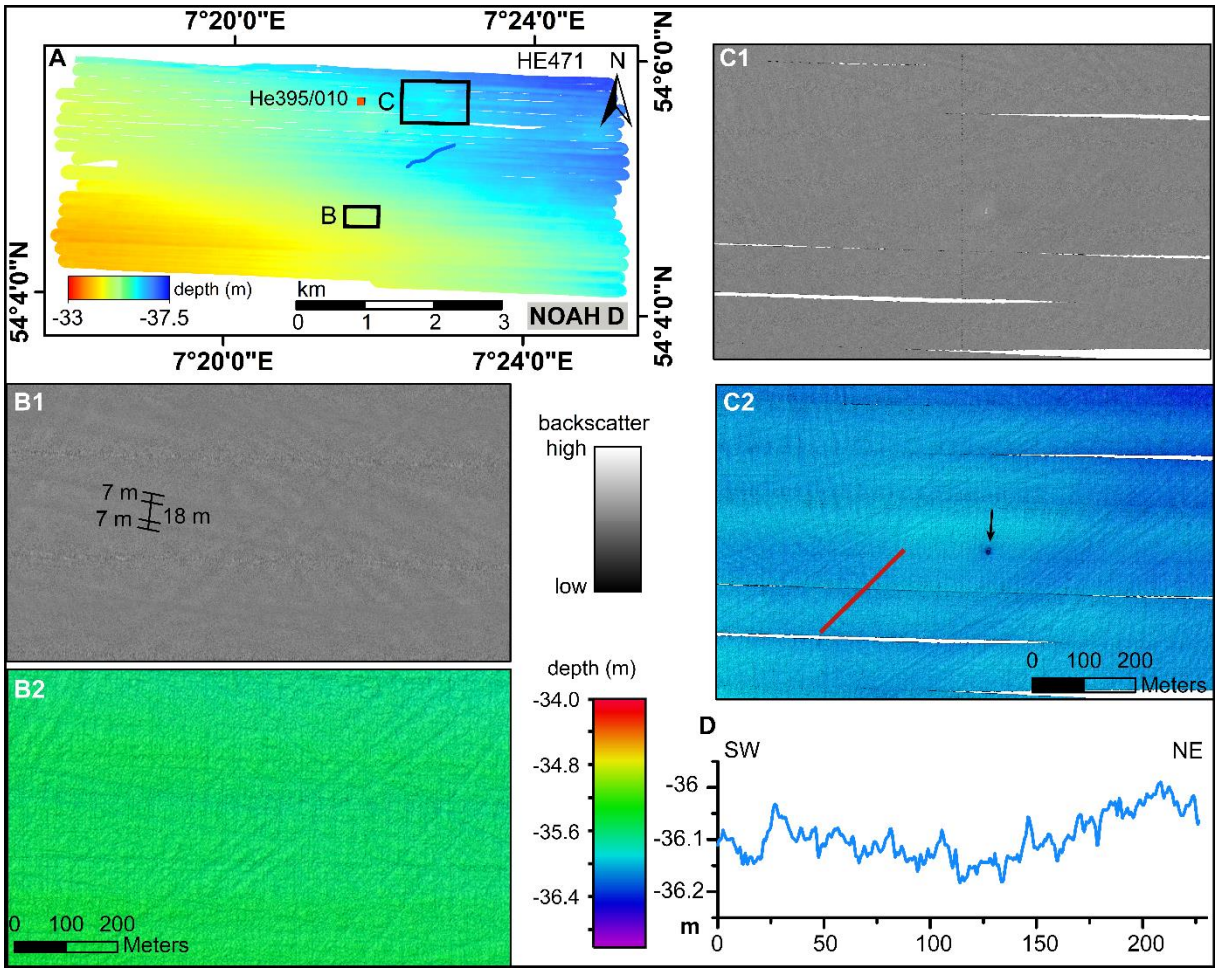

Fig. 9. Multibeam bathymetry of NOAH D (see location Fig. 1) with outline box of enlargements: backscatter (B1, C1) and bathymetry (B2, C2). D) Topographic profile (red line in C2). Black arrow in C2 point to wreck location.

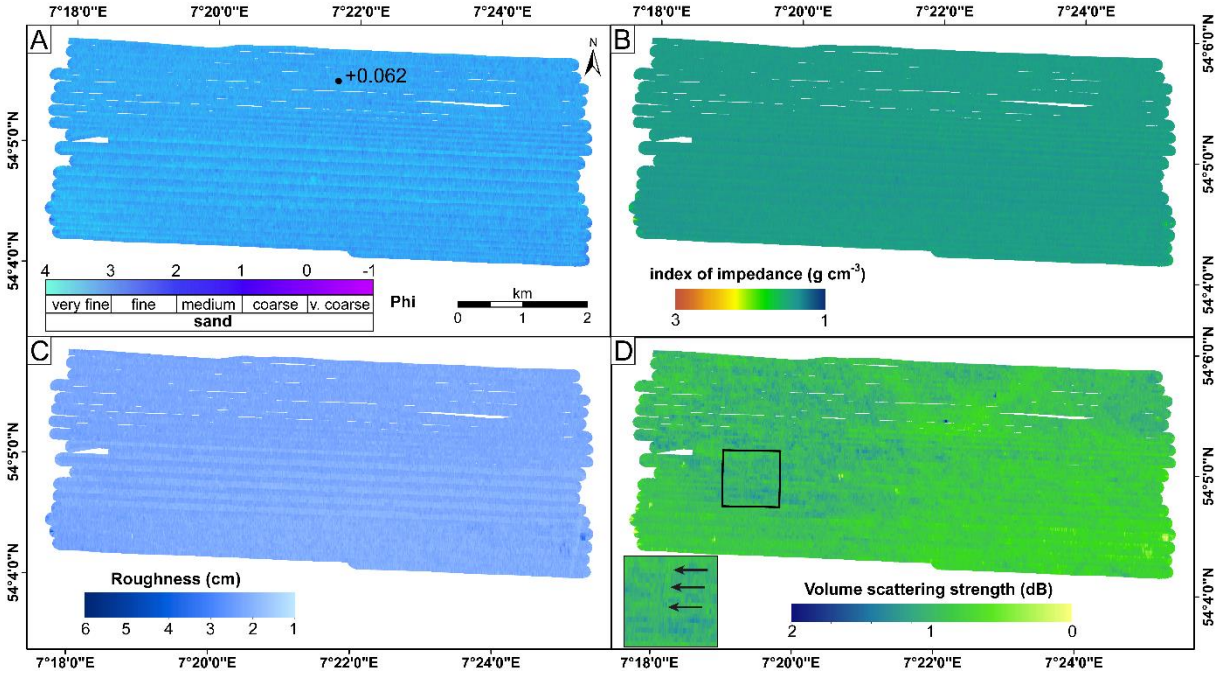

Fig. 10. NOAH D ARA-analysis including grain size (A), index of impedance (B), rms roughness (C) and volume scattering strength (D). Like in NOAH G the beam trawl density is very high and the ARA parameter look relatively homogeneous. Except the volume scatter shows reduced intensities along some of the tracks (black arrow). Black dot indicates sample location. Numbers reveal delta phi (mean grain size) between samples and ARA results.

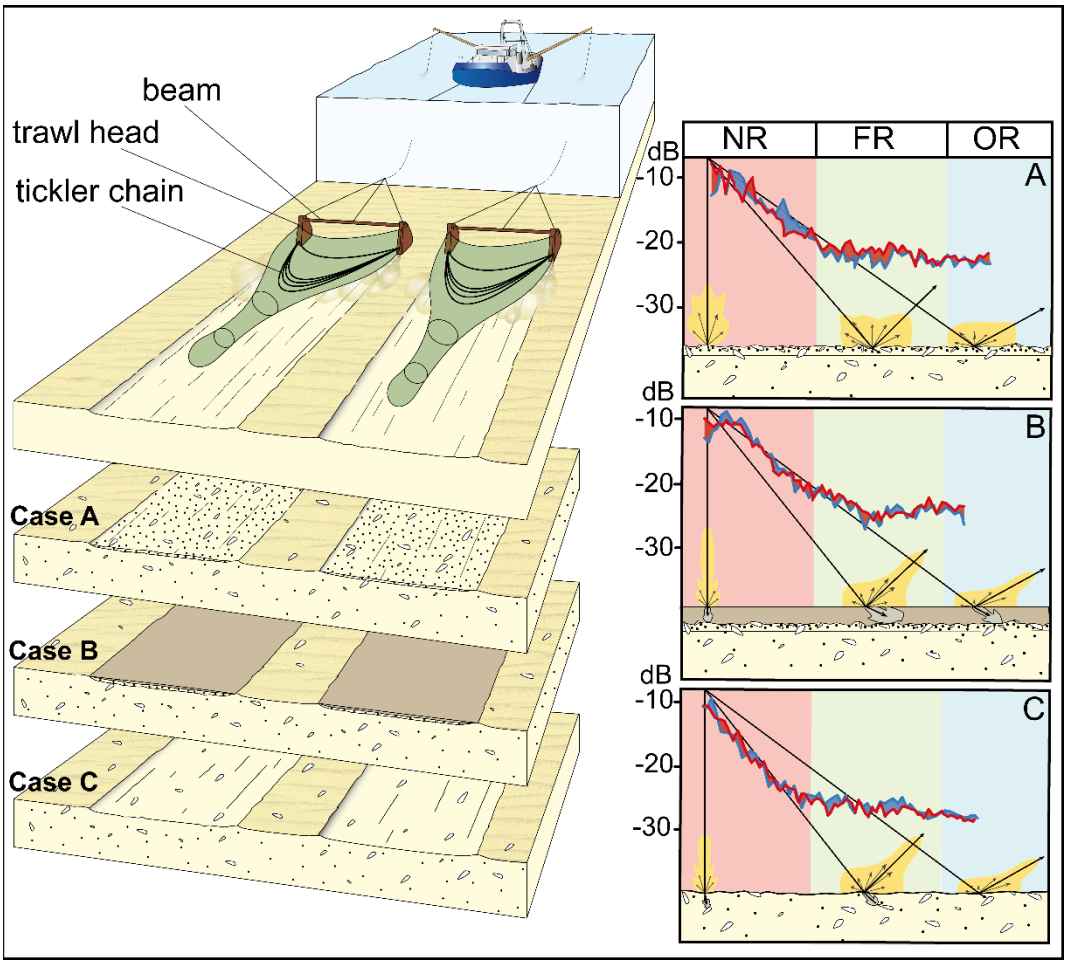

Fig. 11. Model of beam trawl track generation (left) in association with the hydroacoustic pattern. Delineated are three different cases (A, B and C) representing the observations in the three NOAH study areas. On the right side are displayed the associated beam pattern and the near, far and outer range (NR, FR and OR) scattering contribution. The backscatter angular response curve of the prevailing substrate according to the ARA results surround and within the tracks is indicated by the blue and red curve, respectively. Additionally, the area between both curves is colored in red for values greater and in blue for values lower the background backscatter strength. Case A corresponds to the situation in northern part of NOAH I (HE422) with relatively fresh tracks that show a high backscatter strength. Case B demonstrates the situation in the southern part of NOAH I (HE468) with refilled tracks that display as well a high backscatter strength. Case C describes the situation in NOAH D with unfilled tracks that exhibits low backscatter strength (see text for further discussion).

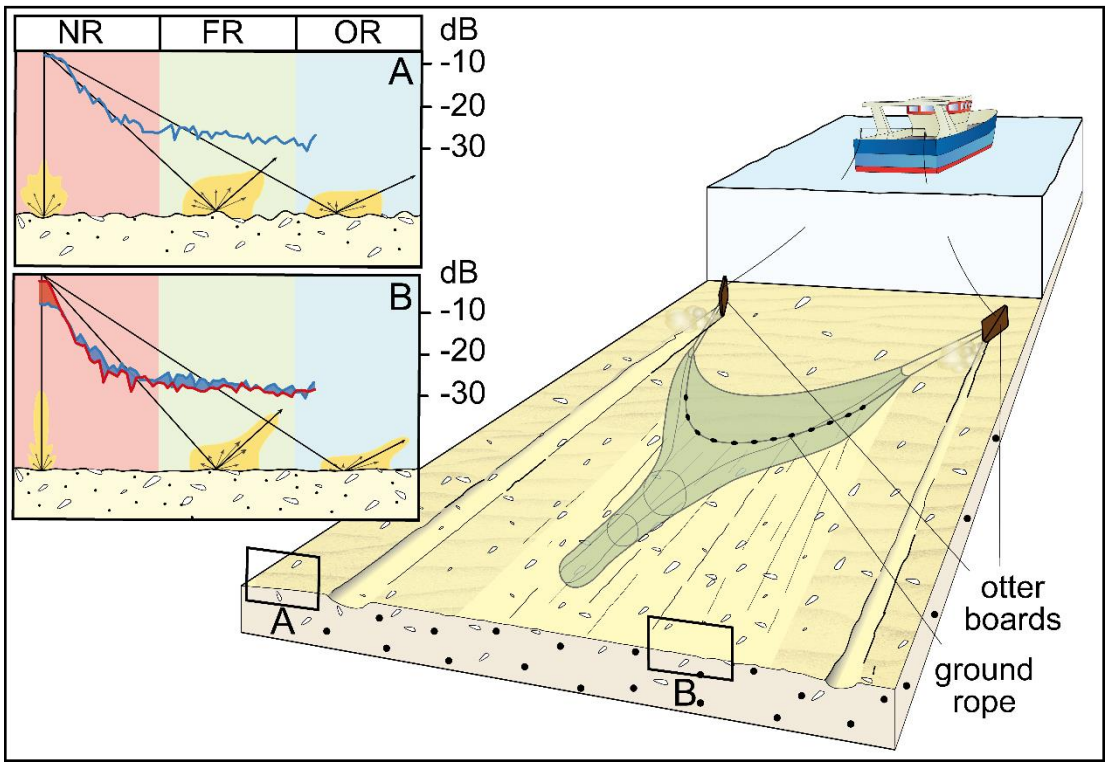

Fig. 12. Model of otter trawl track generation in association with the hydroacoustic pattern. The sketches show the backscatter for the seabed outside (A) and inside (B) the tracks. Demonstrated are the near, far and outer range (NR, FR and OR) scattering pattern observed in NOAH G. The backscatter angular response of the prevailing substrate according to the ARA results outside and within the zone scratched by ground rope is indicated by the blue and red curve, respectively. Additionally, the area between both curves is colored in red for values greater and in blue for values lower the background backscatter strength. It is characterized by high near range backscatter strength and stripes of low backscatter in the far and outer range (see text for further discussion).

Area	**NOAH D**	**NOAH G**		**NOAH I**	
Mean and max. Current Velocity (cm s^{-1})	38.8 (77.0)	19.9 (61.0)		16.6 (73.0)	
Average max. Bed Shear Stress (N m^{-2})	0.20-0.07	0.22-0.04		0.45-0.04	
Cruise	HE471	HE422	HE468	HE422	HE468
Date	Sept. 2016	May 2014	July 2016	May 2014	July 2016
Vessel Speed (kn over ground)	5	4.5	5	4.5	6
Wind Speed (m s^{-1})	5-8	8-10	8	8-11	5-7
Wind Direktion	SSW-W	SSW	W	S	S
EM710 Acquisition Mode	very shallow	shallow	shallow	shallow	shallow
Pulse Length (µm)	200	500	500	500	500
Line Overlap (%)	17	14	18	9	20
Resolution Bathymetry (m)	1	1	1	1	1
Resolution Mosaic (m)	0.27	0.43	0.3	0.33	0.26
Resolution ARA patch (average m^2)	600	1280	1540	1120	780

Table 1 Summary of acquisition and processing parameters.

Area	**NOAH D**	**NOAH G**			**NOAH I**		
Cruise	HE471	HE422	HE468		HE422		HE468
Date	Sept. 2016	May 2014	July 2016		May 2014		July 2016
Dominant Sediment Type	very fine sand	very fine to muddy sand	very fine to muddy sand		very fine sand		fine sand
Shell Fragments	yes	no	no		yes		yes
Track Type	1	1	1	2	1	2(?)	1
Track Density	very high	very high	very high	high	medium	very low	high
Tracks seen in Bathymetry	visible	not visible	visible	visible	visible	not visible	visible less than backscatter
Tracks seen in Backscatter	visible low	visible high	visible high	stripes high/low between tracks	visible high	lower than background at nadir higher	visible high
Tracks seen in ARA (Phi)	not visible	not visible	not visible	coarser between tracks	coarser than background	coarser than background	finer than background
Tracks seen in ARA (Impedance)	not visible	not visible	not visible	high between tracks	higher densities	higher than background	lower densities
Tracks seen in ARA (Roughness)	not visible	not visible	not visible	low between tracks	lower than background	lower than background	lower than background
Tracks seen in ARA (Volume)	visible	not visible	not visible	low between tracks	lower than background	lower than background	higher than background

Table 2 Summary of track characteristics.